CANCER RESEARCH COMMUNICATIONS

AACR American Association for Cancer Research

RESEARCH ARTICLE https://doi.org/10.1158/2767-9764.CRC-25-0259 OPEN ACCESS

Collagen-Bearing Exosomes from Breast Cancer–Associated Fibroblasts Promote T-cell Dysfunction

Samir Jana[1], Matthew Lawton[2], Pin-Ji Lei[3], Harold Hui[1], Andrew Emili[4], and Dennis Jones[1]

ABSTRACT

Cancer-associated fibroblasts (CAF), a major component of the breast tumor microenvironment, drive immune evasion in various cancers by promoting T-cell exclusion and dampening T-cell activation. Previous studies have implicated CAF-derived soluble factors in mediating these immunosuppressive effects. In this study, we investigated whether exosomes secreted by CAFs could suppress T-cell activity. Inhibition of global exosome secretion in breast tumor–bearing mice significantly reduced tumor growth and increased tumor-infiltrating T cells with lower exhaustion marker expression. Conversely, administration of CAF-derived exosomes into tumors produced the opposite effects. Moreover, CAF exosomes associated with T cells *in vivo* and impaired T-cell activation and cytotoxic potential in *ex vivo* assays. Proteomic and biochemical analyses of T cells exposed to CAF exosomes revealed dampened early T-cell receptor signaling. Mass spectrometry identified an extracellular matrix (ECM) signature on CAF exosomes. Depleting type I and type V collagens from CAF exosomes restored T-cell proliferation, whereas overexpression of collagen in cancer cells led to its incorporation into exosomes, which suppressed T-cell activation. These findings suggest that a signaling bridge between CAF exosomes and T cells, mediated by collagen, promotes T-cell dysfunction, contributing to immune evasion in breast cancer.

Significance: Our data provide the first evidence that ECM proteins associate with mouse and human breast CAF-derived exosomes and directly impair T-cell activation and cytotoxicity. These findings suggest that signaling between collagen-rich CAF exosomes and T cells contribute to local and systemic T-cell dysfunction.

Introduction

Cancer-associated fibroblasts (CAF) represent a major component of the breast tumor stroma (1) and are intricately linked to breast cancer mortality. Specifically, CAFs are associated with the exclusion of cytotoxic anticancer T cells from tumors and suppression of their activity (2, 3). The extracellular matrix (ECM), secreted by CAFs and other stromal cells in tumors, is a key driver of immune suppression and correlates with poor outcomes in patients with breast cancer (4–6). Previous studies have shown that the ECM, including collagen, creates a physical barrier that prevents T cells from accessing tumors (7–10). Additionally, collagen was shown to inhibit the proliferation of CD8 T cells, reduce their cytotoxic function against cancer cells (11), and drive resistance to anti–programmed cell death protein 1/programmed death-ligand 1 (PD-1/PD-L1) immune checkpoint therapies (12).

In addition to the secreted ECM, extracellular vesicles and exosomes (small extracellular vesicles ranging from 40 to 160 nm) secreted from CAFs facilitate tumor progression and therapeutic resistance (13, 14). However, most studies on tumor exosome immunomodulation have focused on cancer cell–derived exosomes that can suppress (15, 16) or even kill (17) T cells. More recently, several studies have demonstrated that PD-L1 on cancer cell–derived exosomes binds to PD-1 on cytotoxic CD8 T cells to render them dysfunctional (16, 18–23). Despite the emerging immunomodulatory roles of exosomes in tumor progression, it is unknown whether CAF exosomes directly influence T-cell function. Given that CAFs secrete immunomodulatory cytokines, such as TGFβ and IL10 (13, 24, 25), and that exosomes recapitulate the molecular composition of their cells of origin (26), we questioned whether CAF-derived exosomes could likewise impair T cell–mediated antitumor immunity.

In this study, we demonstrate that human and murine CAF exosomes directly impair T-cell activation and cytotoxic potential. Unbiased mass spectrometry (MS) showed an enrichment of ECM proteins associated with CAF exosomes, and functional studies demonstrated a critical role for

[1]Department of Pathology & Laboratory Medicine, Boston University Chobanian & Avedisian School of Medicine, Boston, Massachusetts. [2]Center for Network Systems Biology, Boston University, Boston, Massachusetts. [3]Edwin L. Steele Laboratories for Tumor Biology, Department of Radiation Oncology, Massachusetts General Hospital, Harvard Medical School, Boston, Massachusetts. [4]Division of Oncological Sciences, Knight Cancer Institute, Oregon Health & Science University, Portland, Oregon.

Corresponding Author: Dennis Jones, Department of Pathology & Laboratory Medicine, Boston University, 670 Albany Street, Room 413, Boston, MA 02118. E-mail: djones1@bu.edu

doi: 10.1158/2767-9764.CRC-25-0259

This open access article is distributed under the Creative Commons Attribution 4.0 International (CC BY 4.0) license.

©2026 The Authors; Published by the American Association for Cancer Research

collagens in suppressing T-cell activity. Together, our data suggest that the ECM on CAF exosomes contributes to the suppression of antitumor T-cell responses.

Materials and Methods

Mice

Female BALB/c mice were purchased from The Jackson Laboratory (cat. #000651, RRID: IMSR_JAX:000651) and entered the studies at 6 to 10 weeks old. Mice were anesthetized with an intraperitoneal injection of a ketamine (100 mg/kg)/xylazine (10 mg/kg) cocktail. All animal studies were reviewed and approved by the Institutional Animal Care and Use Committee of Boston University.

Cell lines and tumor induction

All cells were grown *in vitro* in high-glucose DMEM containing 10% heat-inactivated fetal bovine serum (FBS). Cells were maintained in a 5% CO_2-humidified incubator at 37°C. 4T1 mammary carcinoma (ATCC, CRL-2539; RRID: CVCL_0125), MCa-P1362 (MCaP) mammary adenocarcinoma cells arose spontaneously in a retired breeder, as described previously (27). Authentication information was not provided by the vendor, and no independent testing was conducted on 4T1 or MCaP lines. 4T1 and MCaP cells were maintained and implanted at passages less than 10. 4T1 and MCaP cells were *Mycoplasma*-free (last tested in July 2025 using SouthernBiotech Mycoplasma Detection Kit). Human fibroblasts (gift from Dr. Thomas A. Hughes of the University of Leeds, United Kingdom) were not tested for *Mycoplasma* nor authenticated. For tumor induction, 1×10^5 4T1 cells and 1×10^6 MCaP cells in 50 μL of Hanks' Balanced Saline Solution were implanted into the second mammary fat pad (MFP) of 6- to 10-week-old female BALB/c mice.

Tumor volumes were calculated using the following formula: tumor volume $= (4/3) \times \pi \times (a/2) \times (b/2)^2$.

Collection and culture of lymph node T cells

Naïve T cells were purified from the spleens and lymph nodes of naïve BALB/c mice (The Jackson Laboratory, cat. #000651). For spleen cell preparation, single cells were obtained by crushing the spleen using the flat end of a 1-mL syringe plunger and then passing the suspension through a 70-μm cell strainer. The cells were centrifuged at 2,000 rpm for 5 minutes, and the pellet was incubated with RBC lysis buffer at room temperature for 5 minutes. After lysis, cells were centrifuged again and counted.

For lymph node–derived cells, the nodes were first crushed using the top of a 1-mL syringe plunger and then passed through a 70-μm cell strainer. The cells were subsequently centrifuged and counted.

$CD8^+$ T cells were isolated using $CD8a^+$ T Cell Isolation Kit (Miltenyi, cat. #130-096-543). For every 10^7 cells, 10 μL of antibody cocktail and 40 μL of assay buffer [0.5% BSA in phosphate-buffered saline (PBS)] were added and incubated for 5 minutes at 4°C. Then, 20 μL of magnetic beads and 30 μL of assay buffer were added, followed by a 10-minute incubation at 4°C in the dark. $CD8^+$ T cells were isolated by negative selection using either MS or LS MACS columns.

For mouse *in vitro* T-cell cultures, we used complete RPMI 1640 medium containing L-glutamine supplemented with 10% heat-inactivated FBS, 1x penicillin/streptomycin, 0.2 μmol/L β-mercaptoethanol, 1x nonessential amino acids, and 1x sodium pyruvate with IL2 (10 ng/mL).

Human peripheral blood mononuclear cells (PBMC) were isolated from healthy blood by density gradient centrifugation. First, 15 mL of Ficoll density gradient medium was added to the SepMate tube, and an equal volume of blood sample was diluted with PBS containing 2% FBS and added carefully into the tube. The tube was then centrifuged at 800 × *g* for 20 to 30 minutes with the brake off. Cells were carefully harvested by removing the upper layer and collecting the cells. The isolated PBMCs were then cultured in ImmunoCult-XF (StemCell Technologies, cat. #100-0956) with IL2 (10 ng/mL).

Isolation of CAFs from primary tumors, cell lines, and tissue

Tumors were harvested from BALB/c mice bearing 4T1 and MCaP tumors at 3 and 8 weeks after cancer cell injection, respectively. Tumors were dissected aseptically, minced using a sterile scalpel, and incubated in tumor dissociation solution (Miltenyi Biotec) at 37°C for 30 minutes with continuous shaking. The resulting cell suspension was filtered through a 70-μm cell strainer and centrifuged at 2,000 rpm for 5 minutes at 4°C. The cell pellet was washed once with PBS.

To isolate EpCAM-negative$^{(neg)}$ cells, the cell suspension was incubated with 10 μL of CD326 (EpCAM) MicroBeads (cat. #130-105-958) per 10^7 cells for 15 minutes at 4°C following the manufacturer's protocol. The cells were then passed through an MS MACS column (cat. #130-042-201). The flow-through containing $EpCAM^{neg}$ cells was collected and subjected to a second round of magnetic separation to further enrich the CAFs. EpCAM-positive$^{(pos)}$ cancer cells were eluted from the column using assay buffer. The final flow-through was collected as the CAF-enriched population. CAFs were seeded onto collagen-coated culture dishes for downstream experiments.

The same protocol was applied to isolate cancer cells and CAFs from *in vitro*–cultured 4T1 and MCaP cells and to isolate normal fibroblasts from the MFPs of naïve mice.

Primary human fibroblasts were isolated from infiltrating ductal breast carcinoma (estrogen receptor– and progesterone receptor–positive) after surgery. CAFs were identified as fibroblasts located within tumor tissue and within 2 mm of tumor cells, whereas normal fibroblasts were defined based on their proximity to the nonmalignant epithelium, situated at least 1 cm away from the tumor border. The isolated fibroblast lineage was confirmed by the absence of CK18 and 5B5 expression, and cells were then immortalized using viral transduction with hTERT (28, 29).

Isolation of exosomes from serum and cell supernatant

Precipitation method

Blood samples were drawn retro-orbitally from mice, incubated for 30 minutes at room temperature for clotting, and then centrifuged for 10 minutes at 3,000 rpm at 4°C. Serum was separated and isolated from red blood cells, and exosomes were isolated from the serum using the ExoQuick kit # EXOQ5A-1 (System Biosciences) according to the manufacturer's instructions. First, 100 μL of serum was mixed with 26 μL of ExoQuick solution and incubated at 4°C for 30 minutes. Next, the mixture was centrifuged at 1,500 *g* for 30 minutes at 4°C, and the supernatant was

aspirated. The tubes were recentrifuged to remove trace amounts of fluid and then dissolved in 150 μL calcium- and magnesium-free PBS. Exosome preparations were immediately used for quantification by nanoparticle-tracking analysis (NTA), lysate preparation, and cell treatment.

Exosomes were isolated from the cell supernatants using the ExoQuick TC kit # EXOTC50A-1 (System Biosciences). Donor cells for exosome isolation were seeded in cell culture flasks in DMEM containing 10% exosome-free FBS (Neuromics, cat. #FBS-002). After 48 hours, the medium was collected and spun at 4,000 rpm for 10 minutes to remove cell debris. The supernatant was then passed through a 0.22-μm filter. The supernatants were then mixed with ExoQuick TC solution according to the manufacturer's instructions. Ten milliliters of filtered medium was mixed with 2 mL of ExoQuick TC and incubated at 4°C for overnight. The mixture was then centrifuged at 1,500 × *g* for 30 minutes at 4°C, and the supernatant was aspirated. The tubes were recentrifuged to remove trace amounts of fluid and then dissolved in 200 μL calcium- and magnesium-free PBS. Exosome preparations were immediately used for NTA, protein estimation, lysate preparation, and cell treatment.

Column method

Exosomes were also purified by size-exclusion chromatography on a qEV original column (Izon Science, cat. #ICO-35). After 48 hours of culture in exosome-free medium, the medium was collected in the same way, and then 10 mL of medium was concentrated to 0.5 mL with 100 kD concentrator (Thermo Fisher Scientific). The exosomes were purified by size-exclusion chromatography on a qEV original column.

Density gradient ultracentrifugation

Cell culture supernatants were collected in 29-mL OptiSeal tubes (Beckman Coulter) and cleared of cells and debris by filtration through a 0.4-μm syringe filter before centrifugation. To isolate crude exosome pellets, the filtered culture medium was ultracentrifuged at 120,000 × *g* for 16 hours at 4°C using an MLA-50 rotor (Beckman Coulter). The resulting pellets were resuspended in 5.86 mL of PBS and carefully layered on top of a discontinuous iodixanol gradient composed of 50%, 30%, and 10% solutions prepared in 0.25 mol/L sucrose buffer (containing 1 mmol/L EDTA and 1 mmol/L Tris-HCl, pH 7.4), with 7.71 mL of each concentration.

For serum samples, 0.5 mL of serum was diluted with 1.55 mL PBS, and 2.02 mL of this solution was layered onto the same iodixanol gradient prepared with 2.66 mL of each concentration. Both serum and cell culture supernatant gradients were centrifuged at 120,000 × *g* for 16 hours at 4°C (MLA-50 rotor).

Following ultracentrifugation, gradient fractions were carefully collected: 10 fractions of 1 mL each from serum (F1–F10) and 12 fractions of 2.42 mL each from cell culture supernatants (F1–F12). Fraction densities were calculated based on iodixanol concentrations measured by spectrophotometry at 340 nm, following the manufacturer's protocol. Briefly, 100 μL aliquots of iodixanol standards (5%–50%) and diluted density gradient ultracentrifugation fractions (diluted 1:1 with distilled water) were loaded in triplicate into a 96-well microplate (Thermo Fisher Scientific), and absorbance was read at 340 nm using a Multiskan GO spectrophotometer (Thermo Fisher Scientific). Sample densities were interpolated from the standard curve. For immunoblot analysis, 200 μL aliquots of each isolated fraction (serum and media) were mixed with 60 μL of 6× Laemmli reducing sample buffer (Thermo Fisher Scientific) and heated at 95°C for 5 minutes. Equal volumes were loaded per well for SDS-PAGE and immunoblotting.

After each isolation procedure, the concentration and size of the exosomes were determined before each downstream experiment using a NanoSight NS300 system (Malvern Panalytical).

MS

Samples for proteomic and phosphoproteomic analyses were stored at −80°C until processing. Upon thawing, cells were immediately lysed using guanidine hydrochloride lysis buffer (6 mol/L guanidine hydrochloride, 100 mmol/L pH 8.5 Tris, 40 mmol/L chloroacetamide, and 10 mmol/L TCEP, PhosStop). Bradford assay was performed on each sample to obtain protein concentrations. Protein mixtures were then enzymatically digested using trypsin protease at a 1:50 to 1:100 μg of trypsin: total protein ratio. The lysed samples were digested overnight (16 hours) at 37°C with gentle agitation. The samples were then acidified using a final concentration of 1% formic acid to stop digestion. All samples were then desalted using Sep-Pak desalting columns and dried using a SpeedVac before the peptide concentration was measured using a Pierce peptide quantification assay (Thermo Fisher Scientific, 23275). One hundred micrograms of each sample were labeled using a TMTpro 16-plex kit (Thermo Fisher Scientific, A44520). The samples were pooled after labeling and dried in a SpeedVac. Next, the pooled samples were resuspended in 2% acetonitrile and 0.1% ammonium hydroxide and loaded onto an high-performance liquid chromatograph (HPLC; Agilent 1100). Reversed-phase chromatography was performed with a 53-minute gradient, in which 48 fractions were collected 5 minutes after loading. Every 12th fraction was then pooled and dried for a final total of 12 fractionated samples. Five percent of these were used for proteomic analysis, and the rest were used for phosphopeptide enrichment and subsequent phosphoproteomic analyses.

For phosphoproteomic analysis, fractionated and dried samples were thawed after storage at −80°C on a bench for 5 minutes. Each fraction was resuspended in 800 μL sample buffer (80% acetonitrile and 0.5% trifluoroacetic acid) and spun at 1,600 rpm on a temperature-controlled shaker for 15 minutes at 20°C. The resuspended fractions were loaded into 96-well plates and placed in a KingFisher (Thermo Fisher Scientific) sample purification system. Six other plates were prepared and placed into KingFisher alongside the sample plate: (i) Plate with a comb tip to cover the magnetic rods. (ii) Bead plates containing washed iron beads (10 μL beads/100 μg of peptide, Cube Biotech, 31505-Fe) in wash buffer (80% acetonitrile and 0.1% trifluoroacetic acid). (iii) The first wash plate contained 800 μL of wash buffer. (iv) The second wash plate contained 800 μL of wash buffer. (v) The first elution plate contained 200 μL elution buffer (50% acetonitrile, 7.5% ammonium hydroxide). (vi) The second elution plate contained 200 μL elution buffer. KingFisher was programmed to pick up the phosphoenrichment beads using magnetic rods and incubate them with the samples for 20 minutes with agitation. The beads (now bound with phosphopeptides) were then transferred to the first wash plate and incubated for 5 minutes with agitation and then again to the second wash plate. Finally, the beads were transferred to elution plates and incubated for 5 minutes with agitation. The two

eluates for each fraction were collected and pooled before drying using a SpeedVac.

The prepared samples were stored at −80°C until the mass spectrometer was ready. First, the samples were resuspended in 2% acetonitrile and 0.1% formic acid (mobile phase A) and transferred to a 96-well plate, which was loaded in an Easy nanoLC1200 HPLC system and analyzed using an Exploris 480 with FAIMS Pro (Thermo Fisher Scientific). The peptide mixtures were first loaded into a reversed-phase nanotrap column (75 mm i.d. 3 2 cm, Acclaim PepMap100 C18 3 mm, 100 Å, Thermo Fisher Scientific) and separated by an EASY-Spray column (ES803A, Thermo Fisher Scientific) using a gradient (6%–17% over 77 minutes, then 17%–36% over 45 minutes for peptides, 6%–19% over 58 minutes, then 19%–36% over 34 minutes for phosphopeptides) of mobile phase B (0.1% formic acid and 80% acetonitrile) at a flow rate of 250 nL/minute. The positive ion mode was used throughout, with a capillary temperature of 275°C and spray voltage of 2,100 V. Our DDA method chose the 12 most abundant ions for fragmentation (Exploris 480 NCE 33%), with FAIMS cycling at −50, −57, and −64 V for each full scan. Precursor scans were acquired at 120,000 FWHM resolution with a maximum injection time of 120 milliseconds in the Orbitrap analyzer. The following 0.8 seconds were dedicated to fragmenting the most abundant ions at the same FAIMS compensation voltage, with charge states between 2 and 5, via HCD (NCE 33%) before analysis at a resolution of 45,000 FWHM with a maximum injection time of 60 milliseconds. Phosphopeptides were analyzed in the same manner as the shortened gradient described and an injection time of 150 milliseconds.

Briefly, the protein content of three biological replicates from the three experimental groups was normalized. Trypsin-digested protein fragments were then subjected to hydrophilic interaction liquid chromatography (HPLC) fractionation. A portion of each fraction was used for global proteomic analysis, whereas titanium-coated Sepharose beads were used to enrich phosphopeptides from the remaining sample. Phosphopeptide and peptide mixtures were analyzed using LC/MS. All acquired MS/MS spectra were searched against the UniProt mouse complete proteome FASTA database using the MaxQuant software. A false discovery rate cutoff of 1% was applied to filter the identified candidate peptides and phosphopeptides.

MS analysis

Significantly differentially expressed proteins or phosphoproteins were identified using an adjusted P value cutoff of ≤0.05 and a log (fold change) ≥1. Data visualization was performed using the R packages EnhancedVolcano (v1.22.0) and ComplexHeatmap (v2.20.0). Gene Ontology (GO) annotation and gene set enrichment analysis were conducted using the msigdbr (v7.5.1) and clusterProfiler (v4.12.6) packages in R.

T-cell proliferation assay

Mouse

Cancer cells and CAFs were presorted into $EpCAM^{pos}$ and $EpCAM^{neg}$ populations using anti-mouse CD326 (EpCAM) MicroBeads (Miltenyi, cat. #130-105-958). For T-cell proliferation assays, cell suspensions from mouse lymph nodes or isolated CD8 T cells from lymph nodes or spleens, and human PBMCs were stained with carboxyfluorescein diacetate succinimidyl ester (CFSE; BD Horizon CFSE, cat. #565082, RRID: AB_2869649). A total of 5 to 10 × 10^6 T cells were dissolved in 1 mL PBS, followed by the addition of 0.2 μL of CFSE solution (10 mmol/L) and incubation for 10 minutes at room temperature in the dark. After 10 minutes, 9 mL of complete T-cell medium was added, and the cells were incubated for an additional 5 minutes. Next, the cells were centrifuged and plated in a 24-well plate at a concentration of 2 × 10^5 cells/well, followed by stimulation with 4 μL anti-CD3/CD28 activation beads (Miltenyi, cat. #130-093-627) for mouse. Five microliters of anti-CD3/CD28 activation beads (STEMCELL Technologies, cat. #10971, RRID: AB_2827806) was added to human PBMCs to stimulate T-cell proliferation. Cells were collected after 3 days of culture at 37°C with 5% CO_2.

For experiments that assessed the effects of exosomes from cell-conditioned medium on T-cell proliferation, 10 to 20 μg exosomes were added to 1 × 10^5 cells simultaneously with T-cell activation beads. To investigate the effects of serum exosomes on T-cell proliferation, a ratio of 1.2 × 10^4 exosomes per cell was used.

To assess the involvement of protein phosphatases SHP-1 and SHP-2 on T-cell proliferation in response to exosomes, T cells were pretreated for 30 minutes with the SHP-1 inhibitor TPI-1 (5 μmol/L) or SHP-2 inhibitor SHP099 (10 μmol/L), respectively. Next, 10 μg exosomes were added to 1 × 10^5 cells simultaneously with the T-cell activation beads.

To assess the effects of PD-L1/PD-1 signaling on T-cell proliferation, 10 μg/mL anti–PD-L1 antibody (clone 10F.9G2; cat. #BE0101, RRID: AB_10949073, Bio X Cell) was added to the T-cell cultures 30 minutes before the addition of T cells, activation beads, and/or exosomes.

To measure the effects of rat tail collagen on T-cell proliferation, 100 μg/mL of rat tail collagen (Corning, cat. #CB-40236) was added to CFSE-labeled T-cell cultures along with anti-CD3/CD28 activation beads.

Nucleofection of mouse $CD8^+$ T cells

Mouse naïve $CD8^+$ T cells were isolated from the lymph nodes of female BALB/c mice and activated as described above.

CRISPR RNAs (crRNAs) targeting SHP2, LAIR1, and DDR1 were designed with the Synthego web tool, purchased from Synthego, and reconstituted to 100 μmol/L in TE buffer according to manufacturer's instructions. For preparation of ribonucleoprotein (RNP) complexes, 1.5 μL of each crRNA was combined with 1 μL of Alt-R S.p. Cas9 Nuclease V3 (IDT) and 2.5 μL PBS and then incubated at room temperature for at least 10 minutes. Three days after activation, $CD8^+$ T cells were collected, counted, and 1 × 10^6 cells were resuspended in 82 μL Nucleofector Solution for Mouse T Cells with 18 μL Supplement 2 (Lonza Mouse T Cell Nucleofector Kit, cat. #VPA-1006). Cells were incubated at room temperature for 2 minutes with 5 μL RNP complex, transferred to a nucleofection cuvette, and electroporated using the 2D-Nucleofector Unit (Lonza). Immediately after nucleofection, cells were transferred into prewarmed complete T-cell medium and cultured for 3 days at 37°C. Three days after nucleofection, knockdown efficiency was assessed by immunoblotting cell lysates or cells were labeled with CFSE, as described above, for proliferation assays 72 hours later. Cells undergoing mock nucleofection were subjected to electroporation without the addition of RNP complex.

Generation of ECM scaffolds

Cells were seeded at a density of 1 × 10^4 per well in a glass slide chamber and grown for 5 to 7 days, with the medium being exchanged every 2 days. After

5 days, the medium was aspirated, and the cells were washed with PBS. The cells were then washed three times with 1 mL of prewarmed wash buffer 1 (100 mmol/L Na_2HPO_4, 2 mmol/L $MgCl_2$, and 2 mmol/L EGTA, pH 9.6). Next, 1 mL of prewarmed lysis buffer (8 mmol/L Na_2HPO_4 and 1% NP-40, pH 9.6) was added to each chamber, and the cells were incubated for 15 minutes at 37°C. After this incubation, the lysis buffer was replaced with fresh lysis buffer, and the cells were incubated again for 40 to 60 minutes at 37°C. The lysis buffer was then removed, and the cells were washed five times with 1 mL of wash buffer 2 (10 mmol/L Na_2HPO_4, 300 mmol/L KCl, pH 7.5). Following this, the cells were washed four times with distilled water. After the final wash, distilled water was replaced with either T-cell media/T cells or the decellularized matrix were stained by immunofluorescence.

Flow cytometry analysis

Ex vivo T-cell analysis

To analyze mouse $CD8^+$ and $CD4^+$ T-cell proliferation, CFSE-labeled cells were stained with CD8a-APC antibody (BioLegend, cat. #100712, RRID: AB_312751) and CD4-PE-Cy7 (BioLegend, cat. #100422, RRID: AB_312707). To analyze human $CD8^+$ and $CD4^+$ T-cell proliferation, CFSE-labeled cells were stained with a CD8a-APC antibody (BioLegend, cat. #300911, RRID: AB_314115) and CD4-APC antibodies (BioLegend, cat. #357407, RRID: AB_2565659). The cells were stained for 20 minutes at room temperature, rinsed twice, and analyzed using a BD FACSCalibur flow cytometer (RRID: SCR_000401).

For the analysis of granzyme expression and interferon γ (IFNγ) expression, $CD8^+$ T cells were stained with anti-mouse CD8a-APC antibody for 20 minutes at room temperature. The cells were then washed with PBS, and fixed, and permeabilized using fixation/permeabilization buffer (BD Pharmingen) for 20 minutes at 4°C. The cells were then washed twice with PBS and stained with anti–granzyme B-PE (eBioscience, cat. #12-8898-80, RRID: AB_10853811), anti–IFNγ-PE (eBioscience, cat. #12-7311-81, RRID: AB_466192), or anti–IFNγ-PE/Cy7, (BioLegend, cat. #505825) for 20 minutes at room temperature. The cells were then rinsed twice and analyzed using a BD FACSCalibur flow cytometer (RRID: SCR_000401).

Tissue analysis

High-dimensional full-spectrum flow cytometry was performed using a Cytek Aurora (Cytek, RRID: SCR_027072). Breast tumor tissues were harvested, minced, and digested by incubation at 37°C for 1 hour using tumor dissociation solution (Miltenyi Bioscience, cat. #130-096-730). Lymph node cells were collected as described in the section "Collection and culture of lymph node T cells." Cells were first blocked using TruStain αCD16/CD32 Fc-Block (BioLegend, cat. #101320, RRID: AB_1574975) before staining with a combination of the following antibodies: anti–CD45-Alexa Fluor 532 Invitrogen, cat. #58-0451-80, RRID: AB_11219868; anti–CD3-APC BD Pharmingen, cat. #553066, RRID: AB_398529; anti–CD8-BV 786 BD Horizon, cat. #563332, RRID: AB_2721167; anti–CD4-Alexa Fluor 700, BioLegend, cat. #116021, RRID: AB_2715957; anti-CTLA4 PE CF594, BD Horizon, cat. #564332; anti–LAG3-Brilliant Violet 421, BioLegend, cat. #125221, RRID: AB_2572080; anti–PD-1, Brilliant Violet 510, BioLegend, cat. #135241, RRID: AB_2715761; anti–TIGIT-PE/Cy7, BioLegend, cat. #142107, RRID: AB_2565648 in FACS buffer, and Brilliant Violet Buffer (BD Biosciences). SpectraFlo software (Cytek) was used for spectral unmixing based on UltraComp compensation beads (Thermo Fisher Scientific). All the acquired data were analyzed with FlowJo software (RRID: SCR_008520).

Effect of exosome depletion on tumor growth

MCaP tumor-bearing mice were injected either intratumorally or intraperitoneally with vehicle (5% DMSO) and 2 μg/g (intratumoral) and 2.5 μg/g (intraperitoneal) GW4869 every 2 to 3 days, followed by measurement of tumor size. Intratumoral injection was initiated 33 days after cancer cell implantation, whereas intraperitoneal injection was initiated 3 days after tumor implantation.

Effect of EpCAM-negative exosomes on tumor growth

MCaP tumor-bearing mice were administered either PBS or 20 μg exosomes collected from the supernatant of $EpCAM^{neg}$ cells from the MCaP cell line. Exosomes were injected directly into the tumor at 7-day intervals, and tumor size was measured every 2 to 3 days.

Fluorescent labeling of exosomes with PKH26

Exosomes were labeled with PKH26 dye (Millipore, cat. #PKH26GL) by first resuspending them in 0.5 mL of diluent buffer C provided in the kit. The suspension was then mixed with 2 μL PKH26 dye and incubated for 5 minutes at room temperature. The samples were then mixed with PBS containing 5% BSA and incubated for an additional 5 minutes. To remove any free dye, the samples were then incubated with ExoQuickTC for 60 minutes at 4°C. After this incubation, the samples were centrifuged at 1,500 *g* for 30 minutes at 4°C. The resulting pellets were resuspended in 200 μL of PBS and quantified using the BCA assay (Pierce, Thermo Fisher Scientific). The PKH26-labeled exosomes were then used at a concentration of 10 μg per 1×10^5 cells.

Analysis of T-cell association with exosomes in lymph nodes

To facilitate exosome drainage to the lymph nodes, 20 μg of PKH26-labeled exosomes was subcutaneously injected into the second or fourth MFP of BALB/c mice in a final volume of 50 μL PBS. The control group received 50 μL of PBS. After 24 hours, the mice were sacrificed, and exosome-draining inguinal lymph nodes were harvested for flow cytometry or immunofluorescence analysis.

Association of exosomes with T cells in culture

2×10^5 T cells were seeded into a 24-well plate. On the same day, 20 μg of PKH26-labeled exosomes was added to the cell culture, and the cells were incubated for either 30 minutes or 24 hours. After incubation, the cells were washed three times with PBS, fixed with 4% paraformaldehyde for 10 minutes, and washed three times with PBS. The cells were then stained with anti-CD3 antibody (Abcam, cat. #16669, RRID: AB_443425) overnight, followed by washing thrice with PBS. Next, the cells were stained with Alexa Fluor 488 secondary antibody (Jackson ImmunoResearch Laboratories, 111-545-003, RRID: AB_2338046) for 1 hour. Finally, the cells were mounted using medium containing DAPI and covered with a coverslip.

Depletion of macrophages with clodronate liposomes

The control and clodronate liposomes (clophosomes) were purchased from Formumax Scientific (cat. #NCI1488570). The control liposome solution (30 μL)

was subcutaneously injected into the right footpad of naïve BALB/c mice. Clodronate liposomes were injected into the left footpad of each mouse. Seven days later, 30 μL (containing 30 μg) of MCaP exosomes were injected into the respective footpads. Twenty-four hours later, popliteal lymph nodes were collected for flow cytometry.

Immunofluorescence staining

Mouse lymph nodes were harvested and embedded in optimal cutting temperature compound. Tissues were frozen at −80°C, and 7 to 10 micron frozen sections were cut using a cryostat. Slides from fresh frozen samples were fixed in −20°C acetone for 10 minutes and then allowed to air-dry. For staining of decellularized ECM, cells were grown in culture plates or slide chambers from Electron Microscopy Sciences (cat. #70360-82), fixed with 4% PFA in PBS for 15 minutes at room temperature, and then permeabilized with 0.1% triton-X buffer. To minimize nonspecific antibody binding, tissues or cells were blocked in 5% normal donkey serum for 30 to 60 minutes at room temperature or in 3% BSA in PBS. Anti-mouse CD3 antibody (cat. #ab16669, RRID: AB_443425) was used for staining. Collagen 1A1 (COL1A1) and collagen 5A2 (COL5A2) antibodies used are described below. For nonconjugated primary antibodies, secondary antibodies containing Alexa Fluor nonoverlapping fluorophores (Jackson ImmunoResearch Laboratories), specific to the isotype of the primary antibody, were added.

Western blot

Bradford Protein Assay was used to determine protein concentrations. Protein samples were prepared and boiled for 10 minutes before loading onto 10% Tris-bis-acrylamide gels. Electrophoresis was performed at 100 V for 90 minutes, followed by transfer of the proteins onto a polyvinylidene difluoride membrane at 100 V for 1.5 hours. After the transfer, the membranes were blocked with 5% skim milk in 0.1% Tris-buffered saline with Tween (TBS-T). The membranes were incubated overnight at 4°C on a rotator with primary antibodies diluted in 0.1% BSA in TBS-T. The following primary antibodies were used from Abclonal: CD63, cat. #A21923, RRID: AB_2766090; CD81, cat. #A5270, RRID: AB_2766091; Col1a1, cat. #A22090, RRID: AB_3665644; Albumin, cat. #A0353, RRID: AB_2757141; SHP2, cat. #A12486, RRID: AB_2861667; and LAIR-1, cat. #A23775; DDR1, cat. #A22705. The following primary antibodies were purchased from Proteintech: Alix, cat. #67715-1-Ig, RRID: AB_2882905; anti-calnexin, cat. #10427-2-AP, RRID: AB_2069033; anti-ZAP-70, cat. #60200-1-Ig, RRID: AB_10944567; anti–PD-L1 (cat. #66248-1-Ig, RRID: AB_2756526; and anti–SLP-76, cat. #12728-1-AP, RRID: AB_2136718). The following primary antibody was purchased from Cell Signaling Technology: anti–phospho-Zap70, cat. #2717, RRID: AB_2218658; anti–phospho-SLP-76, cat. #14745, RRID: AB_2798595; anti–phospho-PLCγ1, cat. #14008, RRID: AB_2728690; and anti–E-cadherin, cat. #3195, RRID: AB_2291471. The anti–β-actin antibody was purchased from Millipore Sigma (cat. #A2228, RRID: AB_476697). Anti-COL5A2 antibody (cat. #PA5-14245, RRID: AB_2083084) and anti–ZO-1 (cat. #402200, RRID: AB_2533456) were obtained from Thermo Fisher Scientific. Anti–α-smooth muscle actin was obtained from Abcam (cat. #ab5694, RRID: AB_2223021). Anti–pan-cytokeratin was purchased from Bioss (cat. #bs-1712R, RRID: AB_10855057).

After overnight incubation, the membranes were washed three times with TBS-T for 10 minutes each. Horseradish peroxidase–conjugated secondary antibodies were then applied in 5% skim milk in TBS-T at room temperature for 1.5 hours with rotation. The membranes were subsequently washed three more times with TBS-T (10 minutes each) before being developed using an enhanced chemiluminescence kit (Thermo Fisher Scientific).

For Coomassie staining, equal volumes of samples were loaded into each well and electrophoresed for 90 minutes at 100 V. The gels were then incubated overnight in Coomassie stain with gentle shaking. The next day, gels were destained in destaining solution until the background stain was fully removed and the protein bands were clearly visible. Images were acquired using the iBright imaging system (Thermo Fisher Scientific).

Generation of Cas9-expressing cells

Packaged lentivirus from CELLECTA (pR-CMV-CAS9-2A hygromycin; cat. #SVC99-VS) was used to infect MCaP cells, resulting in MCaP Cas9 cells. Infected cells were sorted using FACS according to GFP expression.

Generation of single-guide RNA–expressing cells

Single-guide RNA (sgRNA) against Rab27a, Col1a1, or Col5a2 was cloned into the pLentiGuide vector (Addgene, item # 117986, RRID: Addgene_117986) with the BsmBI restriction enzyme. Respective vectors were then amplified in Stbl3 bacterial cells and transfected into HEK293T cells (RRID: CVCL_0063) to produce lentivirus, which along with 10 μg/mL polybrene, was then used to transduce MCaP cells that stably expressed Cas9. Cells positive for the Cas9 vector (green fluorescent protein) and sgRNA vector (mCHERRY reporter) were sorted by flow cytometry. The sgRNA sequences were as follows.

Rab27a (forward) 5′- CACCGAACCCAGATATAGTGCTGTG-3′
Rab27a (reverse) 5′- AAACCACAGCACTATATCTGGGTTC -3′
Col1a1 (forward) 5′- CACCGTGTGTATGCAGCTGACTTCA-3′
Col1a1 (reverse) 5′-AAACTGAAGTCAGCTGCATACACAC -3′
Col5a2 (forward) 5′- CACCGCATCTGTCCATGTTGAGTAC-3′
Col5a2 (reverse) 5′-AAACGTACTCAACATGGACAGATGC-3′

As a control comparator, an empty pLentiGuide vector was stably transduced into Cas9-expressing cells.

Generation of CD63, COL1A1, and COL1A2 overexpressing cells

ORF sequences against CD63, COL1A1, and COL1A2 were amplified from the cDNA of $EpCAM^{neg}$ cells using Q5 Taq polymerase (New England Biolabs, cat. #M0491). The amplified sequences were then cloned into the LeGO-iC vector (Addgene, item #27362, RRID: Addgene_27362) using BamH1, EcoRI, and NotI restriction enzymes. To produce lentivirus, the clones were transfected into HEK293T cells with third-generation packaging vectors. The lentivirus-containing medium was then transduced into $EpCAM^{pos}$ cells with 10 μg/mL polybrene. As a control comparator, an empty LeGO-iC was stably transduced into $EpCAM^{pos}$ cells. mCHERRY-positive cells with their respective clones were selected by flow cytometry. The sequences used for cloning are as follows:

CD63 (forward) 5′- CGGGATCCCGCCATGGCGGTGGAAGG-3′
CD63 (reverse) 5′- GGAATTCCCTACATTACTTCATAGCCACTTCG -3′
COL1A1 (forward) 5′- AATGCGGCCGCTGCCATGTTCAGCTTTGTGGACCTC-3′

COL1A1 (reverse) 5′- AATGCGGCCGCTAATTACACGAAGCAG-GCAGG -3′
COL1A2 (forward) 5′- CGGGATCCCGCCATGCTCAGCTTTGTG-GATACG-3′
COL1A2 (reverse) 5′-ATAAGAATGCGGCCGCTAAACTATTTATTT-GAAACAGACGGGGCC -3′

Transmission electron microscopy

The exosome pellets were resuspended and fixed in buffered 2.5% glutaraldehyde. The mixture was then added to a Formvar/carbon film–coated transmission electron microscope grid. After application, the samples were washed with PBS. Images were captured using a JEOL JEM-1011 transmission electron microscope (JEOL, USA Inc.) equipped with an Erlangshen ES100W digital camera (Gatan).

Proteinase K digestion of exosomes

Exosomes were incubated in PBS containing 200 μg/mL proteinase K (Thermo Fisher Scientific, cat. #25530-049) for 1 hour at 37°C. Then proteinase K was neutralized by adding 0.2 μL of boiled 0.2 μmol/L phenylmethylsulfonyl fluoride and incubate for 30 minutes on ice. Exosomes were isolated using the ExoQuick TC kit.

Collagenase I digestion of exosomes

Exosomes (100 μg) were incubated with collagenase at a final concentration of 0.5 mg/mL and 1 mg/mL at 37°C for 30 minutes and subsequently reisolated using the ExoQuick TC kit.

Statistical analyses

Statistical analyses were performed using Prism 9 (GraphPad Software, RRID: SCR_002798). Comparisons between two groups were conducted using two-tailed unpaired Student *t* tests. For experiments involving more than two groups, one-way analysis of variance (ANOVA) was used followed by Tukey honestly significant difference *post hoc* test to correct for multiple comparisons. Tumor growth curves measured longitudinally were analyzed using two-way ANOVA with repeated measures. Statistical significance was defined as $P < 0.05$. All tests were two-sided. Data are presented as the mean ± standard error of the mean (SEM), unless otherwise specified. Sample sizes and numbers of biological replicates are indicated in figure legends.

Results

Breast cancer exosomes promote tumor growth and T-cell exhaustion

Using MCa-P1362 (MCaP) breast cancer (27), we assessed whether exosomes are critical for tumor progression. To this end, MCaP cells were orthotopically implanted into the second MFP of syngeneic BALB/c mice and treated with GW4869, an inhibitor of neuraminidase (30) that blocks exosome secretion (Fig. 1A). Mice were administered intraperitoneal injections of DMSO (vehicle) or GW4869 every 48 to 72 hours for the duration of the experiments. On day 70 aftter implantation, circulating exosomes in the serum of GW4869-treated animals were significantly reduced compared with those in DMSO-treated animals (Fig. 1B). Importantly, exosome depletion significantly inhibited tumor growth (Fig. 1C and D). In a separate study, similar findings were obtained when mice were intratumorally injected with GW4869 (Supplementary Fig. S1).

To understand whether exosomes modulated T-cell responses, primary tumors and tumor-draining lymph nodes were collected on day 70 after implantation (Fig. 1A). Flow cytometric analysis indicated that the frequency of CD8 T cells was elevated in tumor-draining lymph nodes and primary tumors of animals treated with GW4869 relative to vehicle (DMSO) controls (Fig. 1E and F; Supplementary Fig. S2A and S2B). Furthermore, GW4869 treatment reduced the number of CD8 T cells that expressed the exhaustion-associated inhibitory receptors CTLA4, PD-1, LAG3, and TIGIT (Fig. 1E and F). Moreover, exosome depletion led to a higher frequency of cytotoxic CD8 T cells expressing granzyme B and IFNγ in primary tumors (Fig. 1G). Together, these data suggest that breast cancer exosomes may promote tumor progression by suppressing anticancer T-cell responses.

Exosomes associate with T cells *in vitro* and *in vivo*

Next, we tested whether breast tumor exosomes could directly interact with T cells. Exosomes were isolated from cell culture supernatants by precipitation, and their size (mean: 102.3 ± 1.7 nm) was measured by NTA and scanning electron microscopy (Fig. 2A and B). Western blot analysis of exosomes from MCaP and triple negative–like 4T1 breast cancer cells confirmed the presence of exosomal markers CD63, ALG-2 interacting protein X (ALIX), and CD81 (Fig. 2C). As expected, exosomes were negative for the endoplasmic reticulum protein, calnexin. Subsequently, the MCaP exosomes were labeled with the membrane dye PKH26 and incubated with primary T cells from syngeneic BALB/c mice. MCaP exosomes associated with T cells within 30 minutes of incubation (Fig. 2D), and by 24 hours, 89% of anti-CD3/CD28 activated T cells were PHK26+ (Fig. 2E).

Because lymph nodes are a significant reservoir for T cells, we mimicked exosome drainage from the primary tumor to tumor-draining lymph nodes to determine whether exosomes associated with T cells *in vivo*. Exosomes from MCaP cells were labeled with PKH26 and injected into the second MFP of recipient mice. Twenty-four hours after the injection, a fraction of T cells in the draining axillary lymph nodes showed an association with exosomes (Fig. 2F). Exosome colocalization with T cells was significantly increased upon deletion of the subcapsular sinus macrophages with clodronate liposomes (Fig. 2G; Supplementary Fig. S3A and S3B), in agreement with prior studies showing that these macrophages act as a barrier for penetration of tumor extracellular vesicles deep into the lymph node parenchyma (31, 32).

To investigate whether exosomes were transferred to T cells in primary breast tumors, a CD63-mCHERRY reporter construct was generated and stably incorporated into 4T1 breast cancer cells (Fig. 2H). Cells expressing the CD63-mCHERRY construct were injected into the fourth MFP, and parental cells were injected into the corresponding location on the contralateral side. After 2 weeks of cancer growth, T cells isolated from primary breast tumors were analyzed by flow cytometry (Supplementary Fig. S4). A substantial proportion, 35.8% (range, 22.9%–48.7%), of CD8 T cells in the CD63-mCHERRY primary tumors were mCHERRY-positive (Fig. 2H and I). In contrast, only approximately 2% of CD8 T cells in the unlabeled contralateral tumors were mCHERRY-positive. Taken together, these data indicate that breast tumor–derived exosomes interact with T cells within the local tumor microenvironment, with minimal to negligible transfer of exosomes to contralateral tumor sites in this model.

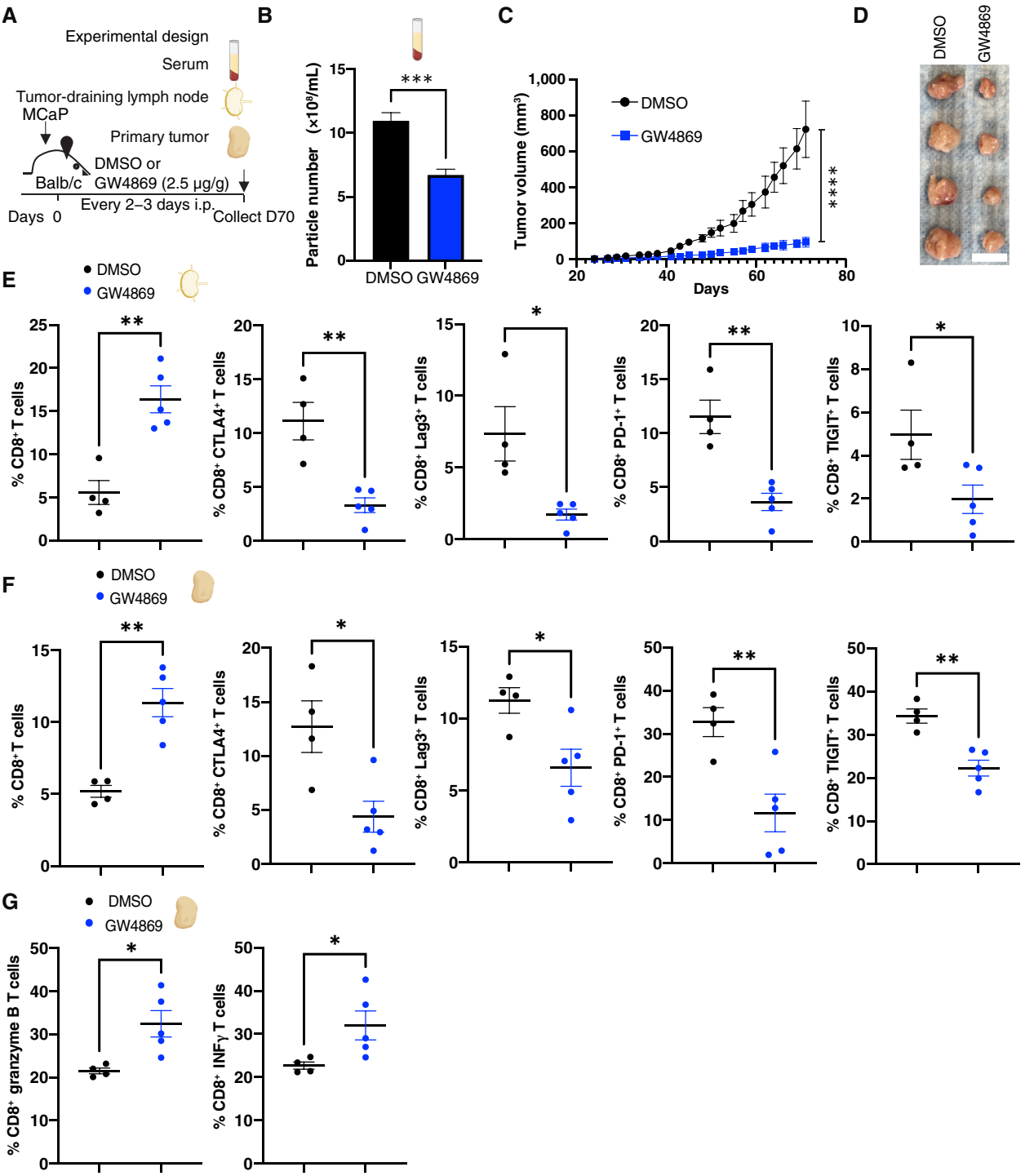

FIGURE 1. Breast cancer exosomes promote tumor growth and T-cell exhaustion. **A,** Schematic design of experimental strategy. **B,** Quantification of serum exosomes during MCaP tumor progression in mice treated intraperitoneally every 2–3 days with DMSO and GW4869 (2.5 μg/g) for 70 days after cancer cell implantation. **C,** Growth curve of MCaP tumors in DMSO- and GW4869-treated mice. **D,** Extracted MCaP tumors from DMSO- and GW4869-treated animals $n = 4$/group. Scale bar, 10 mm. **E,** Quantification and expression of inhibitory receptor expression in CD8 T cells from tumor-draining axillary lymph nodes (**F**) and primary MCaP tumors. $CD8^+$ cells from lymph nodes and primary tumors were gated on $CD3^+$ and $CD45^+$ cells, respectively. **G,** Intracellular expression of granzyme B and IFNγ in CD8 T cells from primary MCaP tumors of DMSO- and GW4869-treated mice. Significance was tested by unpaired Student *t* test (**B** and **E–G**) and two-way ANOVA (**C**). For **B**, **C**, and **E–G**, $n = 4$ (DMSO), $n = 5$ (GW4869) *, $P < 0.05$; **, $P < 0.01$; ***, $P < 0.001$; ****, $P < 0.0001$.

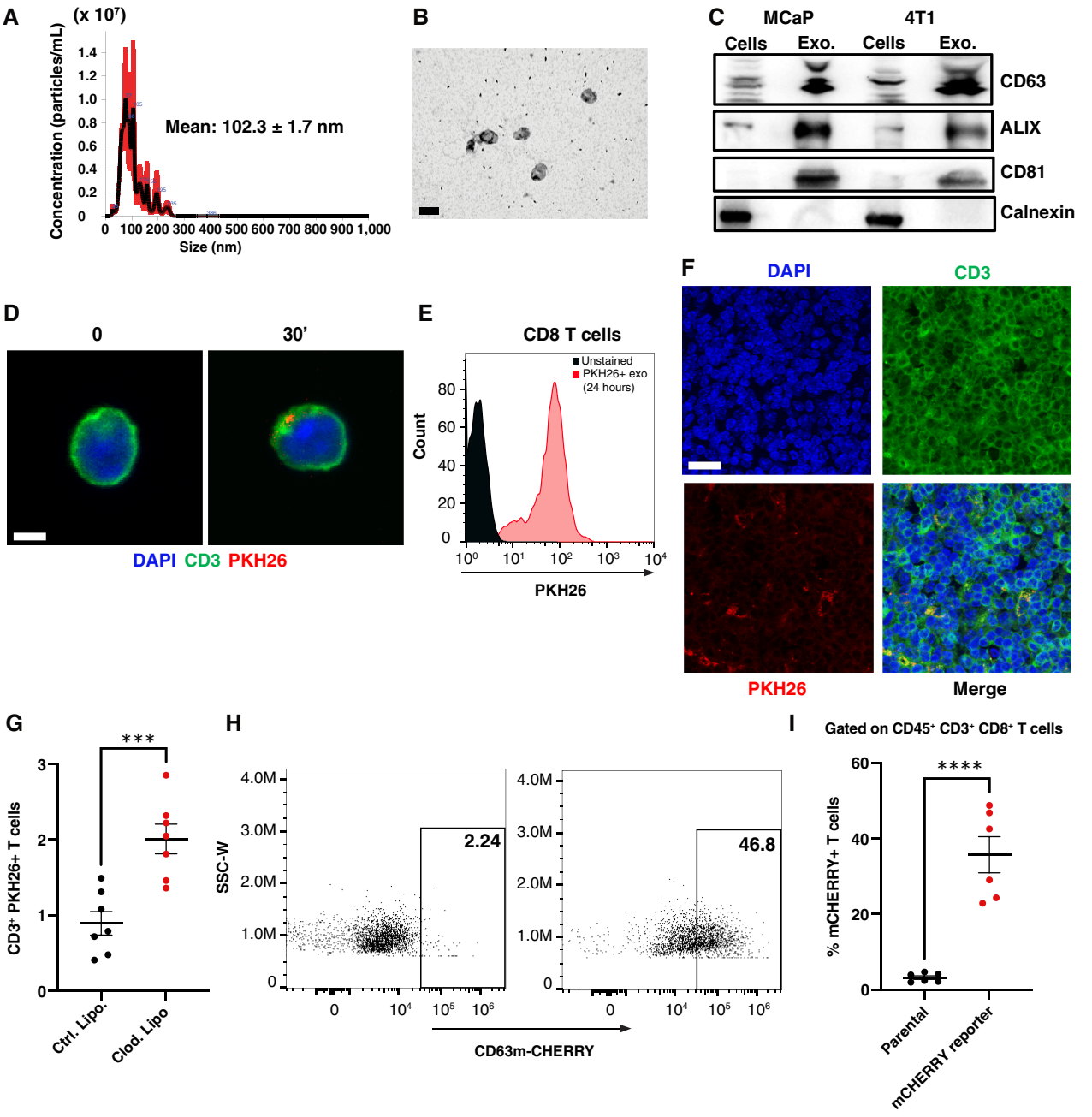

FIGURE 2. T cells associate with breast tumor exosomes *in vitro* and *in vivo*. **A,** Representative NanoSight characterization showing size distribution and concentration of exosomes purified from mammary adenocarcinoma-P1362 (MCaP). Mean (black trace) ± (red trace) SEM data are shown, with the size of the key peaks annotated. **B,** Representative electron microscopy image of MCaP exosomes. Scale bar, 100 nm. **C,** Western blot of indicated proteins from lysates of cells and exosomes (Exo.) from MCaP and 4T1 cancer cells. **D,** Confocal microscopy image of murine T cells incubated for indicated time points with PKH26-labeled exosomes for 30 minutes. Control (0′) shown of left. Scale bar, 2.5 μm. **E,** Flow cytometry to assess PKH26-labeled exosome uptake by CD3/CD28-stimulated CD8 T cells 24 hours after incubation (red shade) compared with untreated T cells (black shade). **F,** 20 μg of PKH26-labeled exosomes (red) were injected into the second MFP of naïve BALB/c mice. After 24 hours, the draining axillary lymph node was fixed, sectioned, and stained with an anti-CD3 antibody to detect T cells (green). DAPI (blue) detects all nucleated cells. Scale bar, 15 μm. **G,** 30 μg of PKH26-labeled exosomes (red) were injected into the footpads of naïve BALB/c mice 6 days after control (right footpad) or clodronate liposome (left footpad) injection. Twenty-four hours after exosome injection, single-cell suspensions from the draining popliteal lymph node were stained with an anti-CD3 APC antibody to detect PKH26+ T cells by flow cytometry. **H** and **I,** On days 14 and 16 after implantation (pooled from two separate experiments), uptake of CD63-mCHERRY exosomes by T cells in primary tumor of mice bearing 4T1 cells transfected with CD63-mCHERRY constructs was measured by flow cytometry. Tumors formed from nontransduced parental 4T1 cells used as a comparator. *P* value calculated by unpaired Student *t* test (**G** and **I**). ***, $P < 0.001$; ****, $P < 0.0001$.

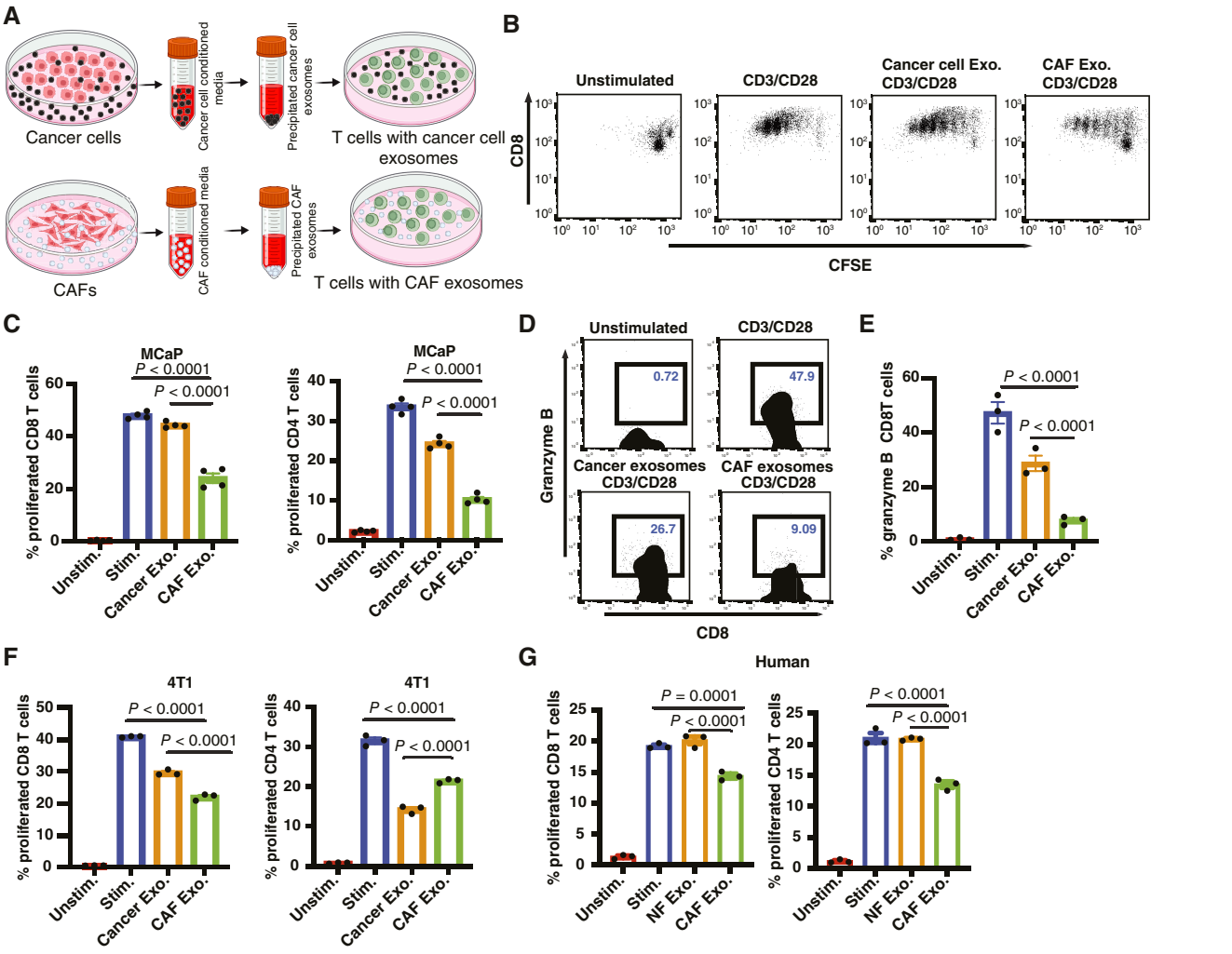

FIGURE 3. CAF exosomes directly inhibit T-cell proliferation. **A,** Schematic of experimental design. **B** and **C,** Proliferation of CFSE-labeled murine T cells 72 hours after concomitant stimulation (Stim.) with anti-CD3/CD28 antibodies and 10 μg/1 × 10^5 cells cancer cell or CAF exosomes (Exo.) from the MCaP line. Unstimulated (Unstim.) T cells used as a negative control. Dot plot of CD8 T cells shown in **B**. Proliferation of gated CD8 and CD4 T cells shown in **C**. **D,** Representative contour plot of granzyme B+ $CD8^+$ T cells in the presence of anti-CD3/CD28 antibodies and cancer cell or CAF exosomes from the MCaP line for 72 hours. Quantification shown in **E**. **F,** Cancer cell or CAF exosomes (10 μg/1 × 10^5 cells) from 4T1 tumor explants were added (10 μg/1 × 10^5 cells) to single-cell suspensions from lymph nodes along with anti-CD3/CD28 antibodies. Proliferation of gated CD8 and CD4 T cells after 72 hours shown. **G,** Exosomes from human normal fibroblasts (NF) or human luminal CAFs were added (10 μg/1 × 10^5 cells) to single-cell suspensions from human PBMCs concomitantly with anti-human CD3/CD28 antibodies. Proliferation of gated CD8 and CD4 T cells shown. Experiments depict three technical replicates from at least three biological replicates. Significance was tested using one-way ANOVA with Tukey honestly significant difference *post hoc* test. [**A,** Created in BioRender. Jones, D. (2026) https://BioRender.com/nbcfuj2.]

CAF exosomes dampen T-cell activation and cytotoxicity

Because of their association with T cells, we next investigated whether breast cancer exosomes could directly regulate T-cell function. Previously, we demonstrated that the MCaP cell line comprises $EpCAM^{pos}$ cancer cells and $EpCAM^{neg}$ CAFs (27). Cancer cells and CAFs were sorted from MCaP tumor explants and showed enrichment in epithelial proteins (cytokeratin and E-cadherin) and mesenchymal proteins (ZO-1 and α-smooth muscle actin), respectively (Supplementary Fig. S5A). Conditioned medium from sorted $EpCAM^{pos}$ and $EpCAM^{neg}$ cells significantly inhibited CD8 T-cell proliferation (Supplementary Fig. S5B), with the medium from $EpCAM^{neg}$ cells exerting a significantly greater inhibitory effect than that from $EpCAM^{pos}$ cells.

Next, we assessed whether exosomes precipitated from conditioned medium could impair T-cell proliferation. To this end, purified exosomes from CAFs or cancer cells were incubated with CFSE-labeled murine T cells (Fig. 3A). Concomitantly, T cells were stimulated with anti-CD3/CD28 antibodies to promote their activation. Flow cytometry revealed that CAF exosomes

significantly limited both CD4 and CD8 T-cell proliferation relative to anti-CD3/CD28–stimulated T cells that were not exposed to exosomes (Fig. 3B and C). Similar to CAF-conditioned medium (Supplementary Fig. S5B), the inhibitory effect of CAF exosomes on CD8 T-cell proliferation was much stronger than that of cancer cell exosomes from the same MCaP tumor explant (Fig. 3B and C). Further analysis demonstrated that significantly fewer $CD8^+$ T cells expressed granzyme B after exposure to CAF exosomes derived from the MCaP cell line (Fig. 3D and E). This limited granzyme B expression suggests CD8 T cells have diminished cytotoxicity upon exposure to CAF exosomes.

To assess whether this effect extended to other breast tumors, cancer cells and CAFs were separated from 4T1 tumor explants based on EpCAM expression. Exosomes derived from both 4T1 cancer cells and CAFs significantly inhibited CD4 and CD8 T-cell proliferation (Fig. 3F). Finally, we grew CAFs from human luminal breast tumor and normal fibroblasts obtained from tumor-adjacent normal tissue (28, 29). Exosomes were isolated from the respective cells and added to CFSE-labeled PBMCs. After 72 hours, CD4 and CD8 T-cell proliferation was significantly decreased in response to luminal CAF exosomes relative to exosomes from normal fibroblasts (Fig. 3G). Collectively, these results underscore the negative regulation of CD4 and CD8 T-cell function by CAF exosomes.

Inhibiting production of CAF exosomes partially restores T-cell proliferation

To confirm that exosomes are required for the inhibitory effects on T-cell proliferation, CAFs were treated with GW4869. NTA confirmed that GW4869 treatment significantly reduced the number of exosomes secreted into conditioned medium (Supplementary Fig. S6A). Importantly, conditioned medium from GW4869-treated cells was less effective than vehicle-treated medium in suppressing T-cell proliferation (Supplementary Fig. S6B). Similar to the effects of GW4869, blocking exosome biogenesis using CRISPR/Cas9 editing of *RAB27A* in CAFs (Supplementary Fig. S6C) reduced exosome production (Supplementary Fig. S6D) and partially reversed the inhibitory effects of the CAF-conditioned medium on T cells (Supplementary Fig. S6E). Together, these data confirm that CAF exosomes contribute to the suppression of T-cell function.

CAF exosomes blunt T-cell receptor signaling

Next, we conducted proteomic analysis to investigate how MCaP exosomes disrupt T-cell function. We first compared unstimulated CD8 T cells with those stimulated with anti-CD3/CD28 antibodies for 48 hours. Differentially expressed proteins, as depicted in volcano plots, revealed enrichment of granzyme B and Slc1a4, a transporter involved in amino acid uptake, in activated CD8 T cells (Fig. 4A). In contrast, other proteins such as Pf4, an inhibitor of T-cell proliferation (33), were elevated in unstimulated T cells. As expected, GO Biological Process analysis showed enrichment of metabolic pathways in the stimulated T cells (Fig. 4B). Next, exosomes from sorted cancer cells or CAFs were incubated with CD8 T cells for 24 hours, followed by stimulation with anti-CD3/CD28 antibodies for 4 hours. CD8 T cells exposed to CAF exosomes had higher expression of ECM-associated proteins (Col1a1 and Col1a2), whereas exposure to cancer cells resulted in the enrichment of proteins involved in metabolism (Cbr2 and Pnpla2), immune cell activation (Ifi44l and C1qtnf1), and proteins expressed in epithelial cells, including Epiplakin 1 and Dsg2 (Fig. 4C). These data suggest that cancer cells and CAF exosomes are incorporated into or bound to CD8 T cells. Importantly, CD8 T cells exposed to CAF exosomes showed reduced small-molecule metabolic pathway activity relative to those exposed to cancer cell exosomes (Fig. 4D).

To directly evaluate alterations in signaling pathways triggered by CAF exosomes, we conducted phosphoproteomic analysis on the same samples to capture global shifts in protein phosphorylation (Fig. 4E). Consistent with proliferation assays (Fig. 3), exposure to CAF exosomes led to reduced activation of proteins involved in cell-cycle progression, including Mki67 and Cdca8. Key components of early T-cell receptor (TCR)-mediated signaling were decreased, including the phosphorylation of phosphatidylinositol-4-phosphate 5-kinase type 1 α (PIP5K1A), a critical enzyme involved in T-cell activation. Phosphorylation of Runx3 and NFATc2, transcription factors that promote the cytotoxic activity of CD8 T cells, also decreased in CD8 T cells exposed to CAF exosomes. Together, these findings suggest that CAF exosomes negatively regulate T-cell activation.

Next, we investigated whether CAF exosomes deregulate the TCR signaling pathways that control metabolism and proliferation. To assess this, CD8 T cells were left unstimulated, or stimulated for 15 or 30 minutes with anti-CD3/anti-CD28 T-cell activation beads, in the presence of cancer cells or CAF exosomes. Phosphorylation of the proximal TCR signaling mediators ZAP-70, SLP-76, and PLC-γ was strongly diminished by CAF exosomes within 30 minutes of bead stimulation (Fig. 4F), suggesting that proteins on the exosome surface interfere with early TCR signaling.

ECM proteins are enriched on CAF exosomes and contribute to T-cell suppression

Because CAF exosomes suppress early TCR signaling, we posited that CAF exosomes dysregulate T cells through surface-to-surface interactions. Recent studies have demonstrated that cancer cell–derived exosomes are enriched with immunosuppressive proteins that dampen T-cell responses, including the immune checkpoint protein PD-L1 (16, 18–23). Exosomes from the MCaP line expressed low levels of PD-L1; however, T cells did not respond to anti–PD-L1 treatment (Supplementary Fig. S7A–S7D). To gain insight into the identity of proteins on the surface of CAF exosomes that could modulate T-cell activity, we eliminated exosomal surface proteins using proteinase K and used proteomics to compare proteinase K–treated CAF exosomes with untreated CAF exosomes (Fig. 5A). Using this subtractive proteomics approach, we found that the most abundant proteins associated with the exosome surface were ECM and ECM-associated proteins (Fig. 5B). The top 10 enriched proteins on CAFs included COL1A1, COL1A2, COL5A2, collagen-binding protein decorin (PGS2), and pigment epithelium-derived factor. Western blotting confirmed the enrichment of COL1A1 and COL5A2 in murine CAFs and their secreted exosomes (Fig. 5C). Blocking exosome secretion with GW4869 resulted in increased levels of COL1A1, COL5A2, and the exosome markers ALIX and CD63 in the cell lysate, whereas their levels decreased in the exosome-enriched fraction (Supplementary Fig. S7E and S7F). The protein expression levels of COL1A1 and COL5A2 in exosomes derived from CAFs were higher than those in exosomes derived from normal fibroblasts obtained from MFPs of naïve mice (Fig. 5C). We observed a similar expression pattern in exosomes

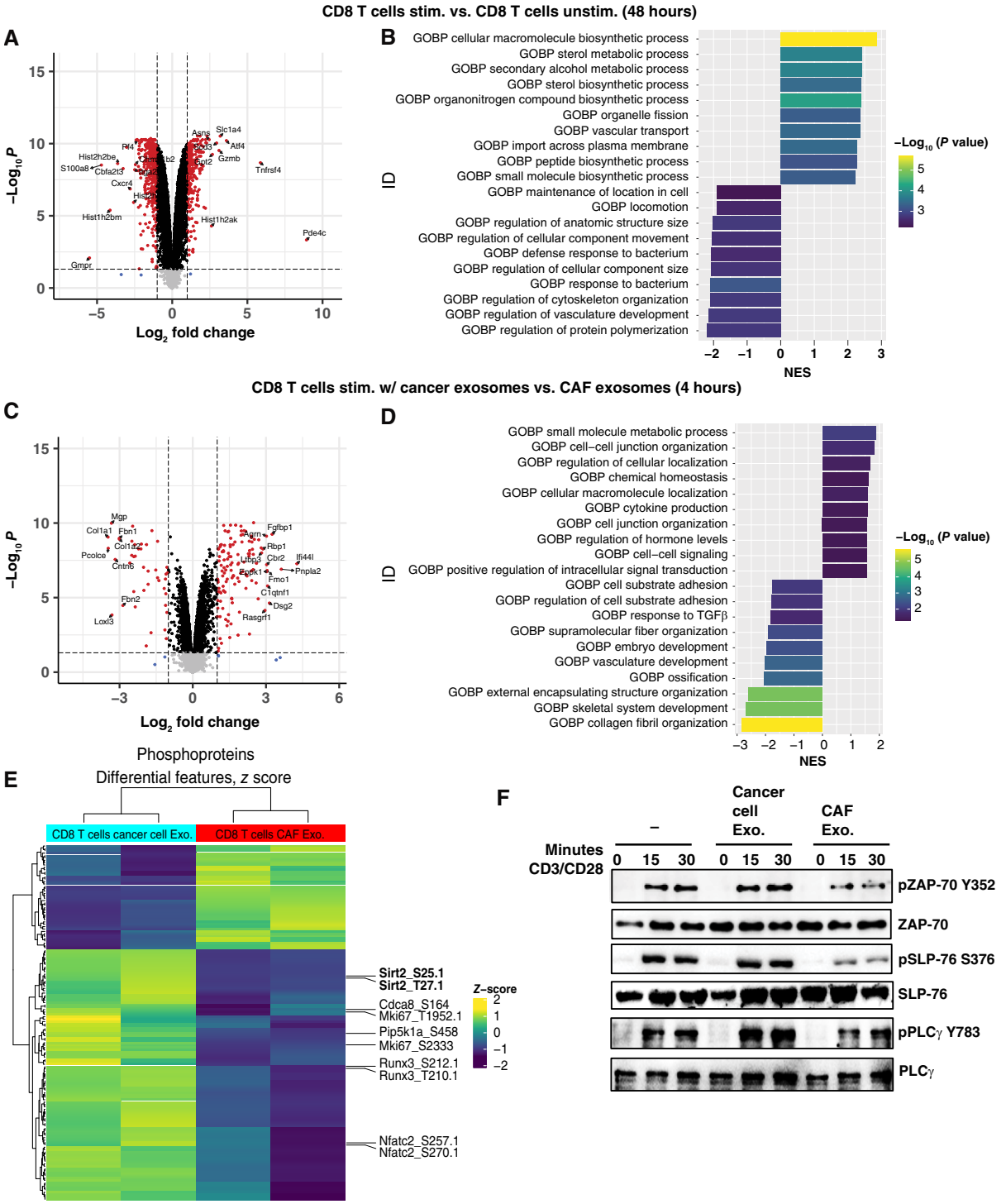

FIGURE 4. CAF exosomes alter TCR signaling, transcriptional regulation, and metabolic profiles in CD8$^+$ T cells. **A,** Differentially expressed proteins were analyzed using volcano plots for comparisons between unstimulated murine CD8 T cells and T cells stimulated with anti-CD3/CD28 antibodies, after 48 hours, with GO Biological Process (GOBP) analysis shown in **B**. **C,** Differentially expressed proteins were analyzed using volcano plots for comparisons between murine CD8 T cells stimulated with anti-CD3/CD28 antibodies for 4 hours, after 24 hours in the presence of cancer cell or CAF exosomes, with GOBP analysis shown in **D**. **E,** Heatmap showing differentially expressed phosphorylated proteins in CD8 T cells exposed to cancer cells or CAF exosomes for 24 hours, followed by stimulated with anti-CD3/CD28 antibodies for 4 hours. **F,** Western blot of phosphorylated (p)ZAP-70 (Y352), total ZAP-70, pSLP-76 (S376), total SLP-76, pPLC-γ (Y783), total PLC-γ in unstimulated (-) CD8 T cells, and CD8 T cells stimulated with cancer cells or CAF exosomes (Exo.) and anti-CD3/CD28 antibodies for 15 minutes or 30 minutes.

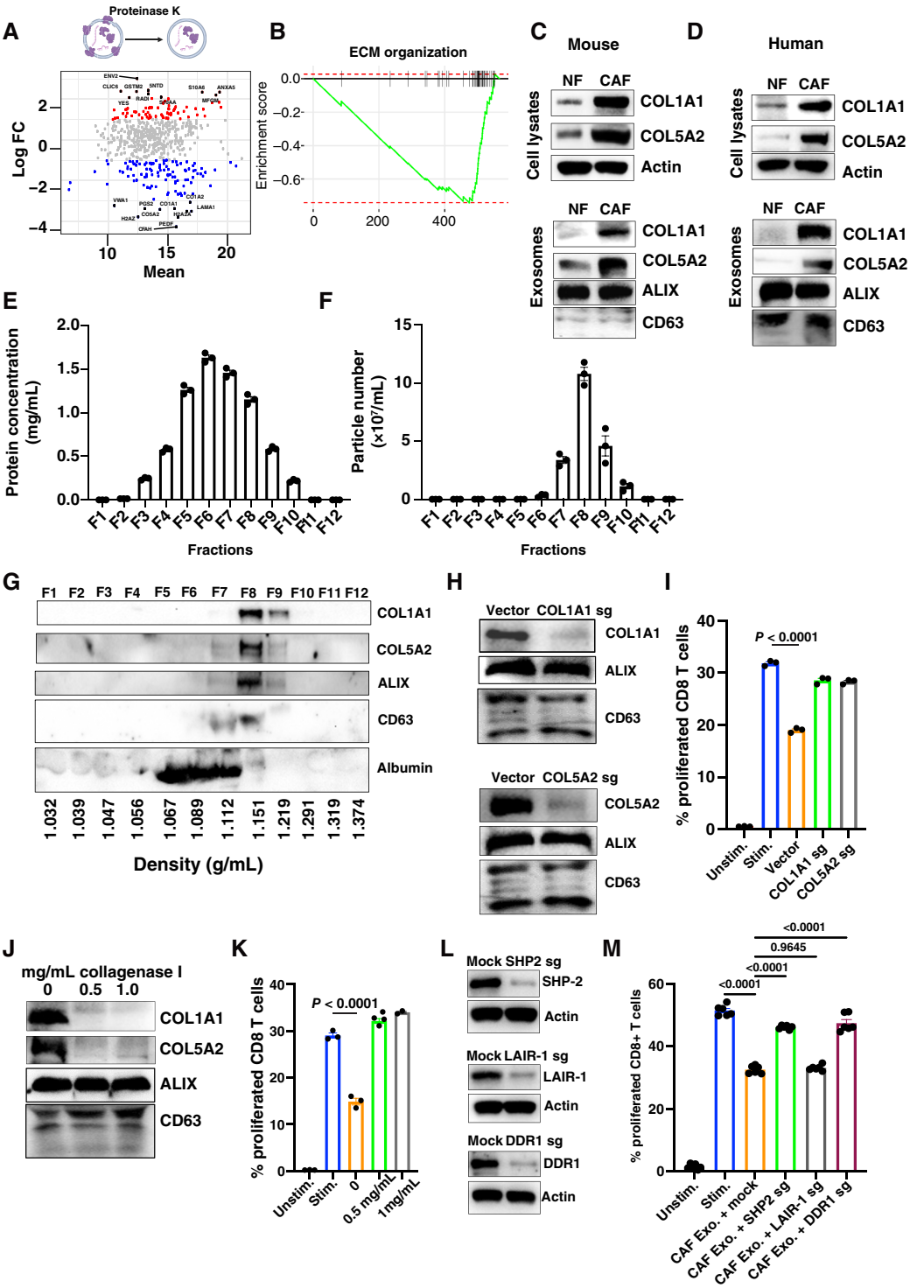

FIGURE 5. Exosomal ECM from CAFs attenuates T-cell proliferation. **A,** Mean difference plot showing the log fold change and average abundance of each protein from CAF exosomes. Proteins with fold changes >1 are highlighted [red, up after proteinase K (PK) or blue, down after PK treatment]. Top 10 labeled. **B,** Gene set enrichment analysis identified proteins associated with ECM organization in CAF exosomes. **C,** Western blot of COL1A1 and COL5A2 proteins in cells (top) and in exosomes (bottom) of normal fibroblasts (NF) from the MFP of naïve animals and CAFs from the MCaP murine cell line. **D,** Western blot of COL1A1 and COL5A2 proteins in cells (top) and in exosomes (bottom) of untransformed normal human fibroblasts (NF) and CAFs from luminal breast cancer. **E** and **F,** Protein content based on BCA assay (**E**) and extracellular vesicle composition (**F**) of fractions 1–12 collected by iodixanol density gradient centrifugation. **G,** Western blot of fractions from (*Continued on the following page.*)

(*Continued*) ultracentrifugation, probed with antibodies against COL1A1, COL5A2, exosome markers Alix and CD63, and the serum protein albumin. **H,** Western blot of COL1A1 (top) and COL5A2 (bottom) in MCaP CAFs with empty vector (vector) or targeted sgRNA (sg) vectors. **I,** Exosomes from MCaP CAFs with empty vector or targeted sgRNA constructs were added to CFSE-labeled T cells along with anti-CD3/CD28 antibodies. CFSE dilution in T cells was measured by flow cytometry 72 hours later. **J,** Western blot of CAF exosomes after collagenase I digestion for 1 hour at indicated concentrations. **K,** CAF exosomes after digestion with collagenase I at indicated concentration were added to CFSE-labeled T cells along with anti-CD3/CD28 antibodies. CFSE dilution was measured by flow cytometry 72 hours later. Significance was tested using one-way ANOVA with Tukey honestly significant difference *post hoc* test (**I** and **K**). **L,** Naïve $CD8^+$ T cells isolated from Balb/c mice were activated with anti-CD3/CD28 antibodies and nucleofected 72 hours later with Cas9 and sgRNAs targeting SHP2, DDR1, or LAIR-1, or with mock nucleofection (mock). Knockdown efficiency was assessed by Western blot. **M,** A subset of T cells from each cohort described in (**L**) was labeled with CFSE and subsequently stimulated with CAF-derived exosomes and anti-CD3/CD28 antibodies. Proliferation was assessed by flow cytometry 72 hours later. CFSE-labeled T cells stimulated with anti-CD3/CD28 antibodies alone served as positive controls (Stim.), whereas unstimulated cells ("Unstim.") served as negative controls. Significance was tested using one-way ANOVA with Tukey honestly significant difference *post hoc* test.

from luminal CAFs and adjacent normal fibroblasts from human breast tumor (Fig. 5D).

We next used ultracentrifugation as an alternative strategy for exosome isolation. The supernatant from CAFs was ultracentrifuged and separated by Optiprep iodixanol density gradient centrifugation. Proteins were detected in all fractions, with enrichment observed in fractions 3 to 10 (Fig. 5E; Supplementary Fig. S8A). NTA analysis showed enrichment of exosomes in fraction 8 (Fig. 5F; Supplementary Fig. S8B). Western blot analysis confirmed the presence of exosomal markers Alix and CD63 in fraction 8 (Fig. 5G). Furthermore, CAF exosomes derived from fraction 8 inhibited T-cell proliferation (Supplementary Fig. S8C), mirroring the effects observed with exosomes isolated using other exosome enrichment methods. Notably, this fraction also contained COL1A1 and COL5A2 (Fig. 5G). Albumin, likely from serum in culture medium, was enriched in nonvesicular fractions. These data provide additional evidence that collagens associate with CAF exosomes.

To investigate the role of COL1A1 and COL5A2 in suppressing T-cell activation, CRISPR/Cas9 was used to delete COL1A1 and COL5A2 in CAFs from MCaP tumors. COL1A1 and COL5A2 knockdown in CAF exosomes was confirmed using Western blotting (Fig. 5H). Exosomes from COL1A1- or COL5A2-depleted cells exhibited a significantly reduced capacity to inhibit CD8 T-cell proliferation (Fig. 5I). As a second method of depleting collagen proteins in exosomes, we subjected exosomes to increasing concentrations of collagenase I. Both COL1A1 and COL5A2 protein levels were reduced after collagenase I treatment (Fig. 5J). Notably, collagenase-digested CAF exosomes were ineffective at suppressing T-cell proliferation (Fig. 5K).

A previous study identified SHP-1 and SHP-2 as key protein phosphatases involved in promoting the development of exhausted CD8 T cells in response to collagen (12). To understand whether SHP-1 and SHP-2 contribute to dysregulated TCR signaling after exposure to CAF exosomes, CD8 T cells were pretreated with the SHP-2 inhibitor SHP099 or the SHP-1 inhibitor TPI-1. Subsequently, CAF exosomes and anti-CD3/CD28 activation beads were concomitantly added to the CD8 T cells. Interestingly, SHP-2 inhibition partially restored the proliferation of CD8 T cells, whereas SHP-1 inhibition did not enhance $CD8^+$ T-cell proliferation (Supplementary Fig. S9A and S9B). We next used electroporation to deliver a CRISPR/Cas9 RNP complex, comprising Cas9 protein and single guide into naïve murine $CD8^+$ T cells to achieve targeted gene deletion. Silencing SHP-2 via CRISPR/Cas9 restored T-cell proliferation in response to CAF-derived exosomes to a degree comparable to that observed with pharmacologic inhibition of SHP-2 (Fig. 5L and M). To investigate which receptor mediated the observed response, we used CRISPR/Cas9 nucleofection to selectively silence the expression of LAIR-1 and DDR1, both of which are receptors that bind collagen (Fig. 5L). Inhibition of DDR1, but not LAIR-1, facilitated T-cell proliferation in response to CAF-derived exosomes (Fig. 5M), Together, these data suggest that CAF exosomes inhibit early TCR signaling, in part through a collagen–DDR1–SHP-2–dependent mechanism.

Next, to test whether exosome collagen is sufficient to enhance T-cell proliferation, we generated MCaP cancer cells that overexpressed COL1A1. As COL1A1 typically exists as a heterotrimer with COL1A2, we also overexpressed both COL1A1 and COL1A2 in cancer cells. Western blot analysis demonstrated the overexpression of COL1A1 and COL1A2 in cancer cells and their exosomes (Fig. 6A). Moreover, compared with the modest inhibition of T cells by MCaP cancer cells, exosomes from cancer cells overexpressing COL1A1 significantly reduced T-cell proliferation (Fig. 6B). The addition of COL1A2 did not further inhibit T-cell proliferation relative to COL1A1 overexpression alone. Exposure of CD8 T cells to exosomes overexpressing COL1A1 led to a significant reduction in the population of activated CD8 T cells expressing granzyme B and IFNγ after anti-CD3/CD28 stimulation (Fig. 6C and D). These data reinforce the role of collagen-containing CAF-derived exosomes in inhibiting T-cell proliferation and cytotoxic function.

Consistent with previous reports, we found that purified rat tail collagen significantly inhibited $CD8^+$ T-cell proliferation (Supplementary Fig. S10A; ref. 11). To further assess the role of collagen in the tumor microenvironment, we generated ECM scaffolds (34) from CAFs isolated from the MCa-P1362 cell line. After 72 hours of contact with the ECM, $CD8^+$ T-cell proliferation was significantly decreased compared with anti-CD3/CD28-stimulated controls (Supplementary Fig. S10B). Using CAF lines with CRISPR/Cas9-mediated knockdown of COL1A1 or COL5A2, we confirmed reduced deposition of these proteins by immunofluorescence (Supplementary Fig. S10C). T cells plated on the ECM from control CAFs showed impaired activation, whereas COL1A1 and COL5A2 depletion partially restored T-cell activation (Supplementary Fig. S10D). These results are consistent with exosome studies demonstrating that COL1A1 and COL5A2 contribute to suppression of T-cell proliferation.

As collagen overexpression in CAF exosomes was sufficient to inhibit T-cell function *in vitro*, we next sought to determine whether this mechanism could modulate tumor progression. First, to measure whether CAF exosomes

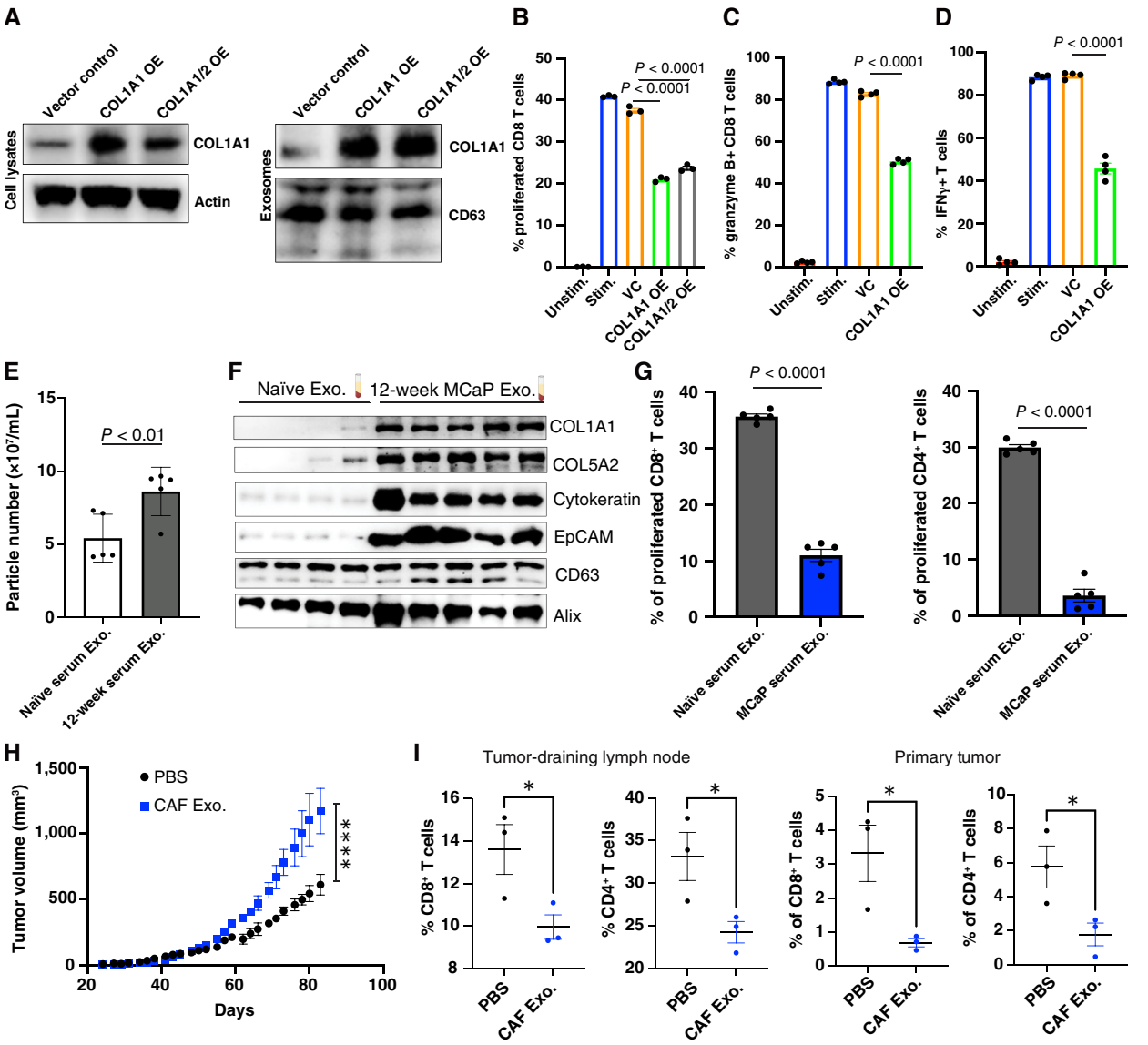

FIGURE 6. ECM from CAF exosomes is critical for attenuating T-cell proliferation. **A,** Western blot of COL1A1 and COL1A2 in MCaP cancer cells (top) and derived exosomes (bottom) from parental cells (transduced with vector control) or cells overexpressing (OE) COL1A1 and or COL1A1/COL1A2 vectors. **B,** Exosomes from MCaP cancer cells expressing vector control (VC), COL1A1, and/or COL1A1/COL1A2 were added to CFSE-labeled T cells along with anti-CD3/CD28 antibodies. CFSE dilution was measured by flow cytometry 72 hours later. **C** and **D,** Exosomes from cohorts in **B** were added to isolated CD8 T cells along with anti-CD3/CD28 antibodies. Flow cytometry measurements of granzyme B (**C**) and IFNγ (**D**) were made after 72 hours. Significance was tested using one-way ANOVA with Tukey honestly significant difference *post hoc* test. **E,** Quantification of serum exosomes during MCaP tumor progression at 12 weeks after implantation. **F,** Western blot analysis of epithelial, ECM, and exosomal marker proteins from purified serum exosomes of tumor-naïve mice ($n = 4$) and mice bearing MCaP tumors ($n = 5$) 12 weeks after implantation. **G,** Single-cell suspensions from lymph nodes of naïve BALB/c mice were incubated for 72 hours with serum exosomes from tumor-naïve mice and mice bearing MCaP tumors 12 weeks after implantation. Flow cytometry was performed to measure the percentage of CD8 (left) and CD4 (right) T cells proliferating in response to concomitant exosome and anti-CD3/CD28 antibody stimulation. **H,** Growth curve of MCa-P1362 tumors injected weekly with PBS or 20 μg weekly of CAF exosomes. **I,** Quantification of CD8 (left) and CD4 (right) T cells in tumor-draining lymph nodes and primary tumors of PBS-injected and CAF exosome–injected mice. *P* value calculated by unpaired Student *t* test (**E**, **G**, and **I**) and two-way ANOVA (**H**). *, $P < 0.05$; ****, $P < 0.0001$.

were elevated during tumor progression, we profiled exosomes from the serum of both tumor-naïve mice and those harboring advanced MCaP tumors at 12 weeks after implantation. Mice bearing MCaP tumors exhibited a significant increase in the overall number of serum exosomes (Fig. 6E). In tumor-naïve mice, the average particle count was 5.4×10^7 particles/mL, whereas in mice with advanced tumors, this count increased to 8.6×10^7

particles/mL. Western blotting showed that the presence of epithelial cell markers, distinguished by the presence of EpCAM, E-cadherin, and cytokeratin, was increased in serum, suggesting that exosomes from breast cancer cells are released systemically (Fig. 6F). In addition, COL1A1 and COL5A2, likely from CAF exosomes, were also enriched in exosomes recovered from the serum (Fig. 6F). Similarly, COL1A1 and COL5A2 were enriched in the exosome-containing fractions isolated from the serum of tumor-bearing mice using density gradient ultracentrifugation (Supplementary Fig. S11A–S11C). We then stimulated CD8 T cells with anti-CD3/CD28 antibodies in the presence of serum exosomes to evaluate their potential immunomodulatory effects. We found that serum exosomes from tumor-bearing mice significantly decreased CD8 and CD4 T-cell proliferation (Fig. 6G).

To assess whether CAF exosomes modulate tumor growth, MCaP cells were implanted into the second MFP of recipient mice, which received weekly intratumoral injections of CAF exosomes or PBS. CAF exosome injections resulted in a significant increase in tumor volume compared with that in mice injected with PBS (Fig. 6H).

Furthermore, using flow cytometry, we observed a significant decrease in the frequency of CD8 and CD4 T cells in tumor-draining lymph nodes and primary tumors of animals injected with CAF exosomes relative to PBS-injected controls (Fig. 6I).

Collectively, these findings establish that CAF-derived exosomes contribute to suppression of T-cell function in breast tumors.

Discussion

CD8 T cells are susceptible to apoptosis and suppression of activation by cancer cell–derived exosomes that present FasL and PD-L1 on their surface (16, 18–23, 35) and contain galectin within their vesicles (36). Thus, the mechanisms of exosome-mediated T-cell suppression are heterogeneous and likely driven by the distinct exosomal contents of different cancer cell types. The influence of breast CAF-derived exosomes on T-cell activity in breast tumors remains largely unexplored.

Collagen I and other ECM proteins have been shown to inhibit T-cell proliferation (11, 37–39). Our data herein suggest that the ECM on CAF exosomes represents a previously unknown mechanism of T-cell suppression. In our model, collagen-induced T-cell exhaustion occurs via an DDR1–SHP-2–dependent mechanism. Moreover, CAF exosomes may engage with and inhibit T cells at multiple interfaces, including within the tumor microenvironment, tumor-draining lymph nodes, and in blood. This is reflected by an exhausted phenotype, reduced proliferative and functional capacity, and impaired ability to constrain tumor growth, all of which were measured in this study. The low percentage of T cells in lymph nodes that colocalize with subcutaneously injected exosomes may reflect limited access to T cells, although the association was enhanced upon depletion of sinusoidal macrophages in lymph nodes. Although the serum of mice with advanced breast cancer was enriched in ECM proteins and demonstrated the capacity to directly inhibit T-cell activation, we cannot exclude the possibility that contaminating serum proteins (based on albumin detection in exosome preparations) may be present and modulate T-cell activation.

Although collagen is necessary to inhibit T-cell activation by CAF exosomes, it is unclear whether collagen also acts as a scaffold for other ECM or immunomodulatory proteins that engage T cells. Interestingly, depleting either COL1A1 or COL5A2 from CAF exosomes restored T-cell proliferation, and knocking down COL1A1 reduced COL5A2 levels, and *vice versa*, suggesting a potential interdependence between these proteins. The DDR1 receptor binds fibrillar collagens, including type I and type V collagens, and thus T cell DDR1 may be critical for binding multiple collagens associated with CAF exosomes. Furthermore, we showed that overexpression of collagen I in cancer cells and their secreted exosomes is sufficient to blunt T-cell proliferation. Thus, it is plausible that ECM produced by cancer cells, particular those with a mesenchymal phenotype, may also inhibit T-cell proliferation.

A limitation of this study is that it did not assess CAF heterogeneity (40), although myCAFs are known to be the main contributors to collagen synthesis in breast tumors. In addition, our experimental approach does not include a CAF-specific knockout of exosome production, which would provide specificity, as GW4869 treatment broadly inhibits exosome secretion across all cell types. Finally, the precise mechanism by which collagen associates with exosomes remains unclear; it is unknown whether collagen binds to exosomes after secretion or is incorporated during exosome biogenesis.

Key findings from the present study indicate that ECM proteins are enriched on exosomes from mouse and human breast CAFs and that these exosomes are associated with and suppress T-cell activation. Thus, in addition to the impact of collagen density and alignment on T-cell migration into tumors (10), data from the current study suggest that targeting collagen-enriched CAF-derived exosomes may also limit the dysfunction of anticancer T cells. Given that exosomal biosignatures can serve as useful noninvasive diagnostic tools (23), further studies are warranted to determine whether elevated levels of collagen in the serum of tumor-bearing mice, as was measured in this study, could provide diagnostic insights into therapeutic response and disease progression for patients with breast cancer.

Data Availability

The MS proteomics data have been deposited to the ProteomeXchange Consortium via the PRIDE partner repository with the dataset identifier PXD074262. Other data generated in this study are available upon request from the corresponding author.

Authors' Disclosures

P.-J. Lei reports grants from Massachusetts General Hospital during the conduct of the study. A. Emili reports grants from the NIH and that A. Emili is the cofounder of Prisma Therapeutics. D. Jones reports grants from the NIH, the American Association for Cancer Research, and the Breast Cancer Research Foundation during the conduct of the study. No disclosures were reported by the other authors.

Authors' Contributions

S. Jana: Data curation, formal analysis, methodology, writing–review and editing. **M. Lawton:** Data curation, formal analysis, methodology, writing–review and editing. **P.-J. Lei:** Data curation, formal analysis, methodology, writing–review and editing. **H. Hui:** Data curation. **A. Emili:** Resources,

supervision, writing–review and editing. **D. Jones:** Conceptualization, resources, data curation, formal analysis, supervision, funding acquisition, writing–original draft, project administration, writing–review and editing.

Acknowledgments

The authors thank Dr. Hui Chen for assistance with scanning electron microscopy. The authors thank the Boston University Flow Cytometry Core Facility for their technical support. This work was supported by the Shamim and Ashraf Dahod Breast Cancer Research Center, 2022 Breast Cancer Research Foundation–AACR Career Development Awards to Promote Diversity and Inclusion, grant number 22-20-26-JONE, Breast Cancer Research Foundation Grant NXTGN-25-007, and National Institutes of Health R01CA284133 to D. Jones. P.-J. Lei was supported by the Massachusetts General Hospital Executive Committee on Research Fund for Medical Discovery (GR1000318). S. Jana was supported by a Shamim and Ashraf Dahod International Scholar Award. A. Emili was supported by the U01CA243004. The authors are solely responsible for providing this information. Funders had no role in the study design, data collection, analysis, interpretation, manuscript writing, or decision to submit for publication.

Note

Supplementary data for this article are available at Cancer Research Communications Online (https://aacrjournals.org/cancerrescommun/).

Received May 13, 2025; revised November 18, 2025; accepted February 16, 2026; posted first February 19, 2026.

References

1. Mao Y, Keller ET, Garfield DH, Shen K, Wang J. Stromal cells in tumor microenvironment and breast cancer. Cancer Metastasis Rev 2013;32:303–15.
2. Schoppmann SF, Berghoff A, Dinhof C, Jakesz R, Gnant M, Dubsky P, et al. Podoplanin-expressing cancer-associated fibroblasts are associated with poor prognosis in invasive breast cancer. Breast Cancer Res Treat 2012;134:237–44.
3. Surowiak P, Murawa D, Materna V, Maciejczyk A, Pudelko M, Ciesla S, et al. Occurence of stromal myofibroblasts in the invasive ductal breast cancer tissue is an unfavourable prognostic factor. Anticancer Res 2007;27:2917–24.
4. Conklin MW, Eickhoff JC, Riching KM, Pehlke CA, Eliceiri KW, Provenzano PP, et al. Aligned collagen is a prognostic signature for survival in human breast carcinoma. Am J Pathol 2011;178:1221–32.
5. Acerbi I, Cassereau L, Dean I, Shi Q, Au A, Park C, et al. Human breast cancer invasion and aggression correlates with ECM stiffening and immune cell infiltration. Integr Biol (Camb) 2015;7:1120–34.
6. Maller O, Drain AP, Barrett AS, Borgquist S, Ruffell B, Zakharevich I, et al. Tumour-associated macrophages drive stromal cell-dependent collagen crosslinking and stiffening to promote breast cancer aggression. Nat Mater 2021;20:548–59.
7. Salmon H, Franciszkiewicz K, Damotte D, Dieu-Nosjean MC, Validire P, Trautmann A, et al. Matrix architecture defines the preferential localization and migration of T cells into the stroma of human lung tumors. J Clin Invest 2012;122:899–910.
8. Peranzoni E, Rivas-Caicedo A, Bougherara H, Salmon H, Donnadieu E. Positive and negative influence of the matrix architecture on antitumor immune surveillance. Cell Mol Life Sci 2013;70:4431–48.
9. Winkler J, Abisoye-Ogunniyan A, Metcalf KJ, Werb Z. Concepts of extracellular matrix remodelling in tumour progression and metastasis. Nat Commun 2020;11:5120.
10. Jones D, Wang Z, Chen IX, Zhang S, Banerji R, Lei PJ, et al. Solid stress impairs lymphocyte infiltration into lymph-node metastases. Nat Biomed Eng 2021;5:1426–36.
11. Kuczek DE, Larsen AMH, Thorseth M-L, Carretta M, Kalvisa A, Siersbaek MS, et al. Collagen density regulates the activity of tumor-infiltrating T cells. J Immunother Cancer 2019;7:68.
12. Peng DH, Rodriguez BL, Diao L, Chen L, Wang J, Byers LA, et al. Collagen promotes anti-PD-1/PD-L1 resistance in cancer through LAIR1-dependent $CD8^+$ T cell exhaustion. Nat Commun 2020;11:4520.
13. Sahai E, Astsaturov I, Cukierman E, DeNardo DG, Egeblad M, Evans RM, et al. A framework for advancing our understanding of cancer-associated fibroblasts. Nat Rev Cancer 2020;20:174–86.
14. Teixeira AF, Wang Y, Iaria J, Ten Dijke P, Zhu HJ. Extracellular vesicles secreted by cancer-associated fibroblasts drive non-invasive cancer cell progression to metastasis via TGF-beta signalling hyperactivation. J Extracell Vesicles 2025;14:e70055.
15. Whiteside TL. Exosomes and tumor-mediated immune suppression. J Clin Invest 2016;126:1216–23.
16. Poggio M, Hu T, Pai CC, Chu B, Belair CD, Chang A, et al. Suppression of exosomal PD-L1 induces systemic anti-tumor immunity and memory. Cell 2019;177:414–27.e13.
17. Andreola G, Rivoltini L, Castelli C, Huber V, Perego P, Deho P, et al. Induction of lymphocyte apoptosis by tumor cell secretion of FasL-bearing microvesicles. J Exp Med 2002;195:1303–16.
18. Chen G, Huang AC, Zhang W, Zhang G, Wu M, Xu W, et al. Exosomal PD-L1 contributes to immunosuppression and is associated with anti-PD-1 response. Nature 2018;560:382–6.
19. Fan Y, Che X, Qu J, Hou K, Wen T, Li Z, et al. Exosomal PD-L1 retains immunosuppressive activity and is associated with gastric cancer prognosis. Ann Surg Oncol 2019;26:3745–55.
20. Ricklefs FL, Alayo Q, Krenzlin H, Mahmoud AB, Speranza MC, Nakashima H, et al. Immune evasion mediated by PD-L1 on glioblastoma-derived extracellular vesicles. Sci Adv 2018;4:eaar2766.
21. Yang Y, Li CW, Chan LC, Wei Y, Hsu JM, Xia W, et al. Exosomal PD-L1 harbors active defense function to suppress T cell killing of breast cancer cells and promote tumor growth. Cell Res 2018;28:862–4.
22. Monypenny J, Milewicz H, Flores-Borja F, Weitsman G, Cheung A, Chowdhury R, et al. ALIX regulates tumor-mediated immunosuppression by controlling EGFR activity and PD-L1 presentation. Cell Rep 2018;24:630–41.
23. Theodoraki MN, Yerneni SS, Hoffmann TK, Gooding WE, Whiteside TL. Clinical significance of PD-$L1^+$ exosomes in plasma of head and neck cancer patients. Clin Cancer Res 2018;24:896–905.
24. Costa A, Kieffer Y, Scholer-Dahirel A, Pelon F, Bourachot B, Cardon M, et al. Fibroblast heterogeneity and immunosuppressive environment in human breast cancer. Cancer Cell 2018;33:463–79.e10.
25. Galland S, Stamenkovic I. Mesenchymal stromal cells in cancer: a review of their immunomodulatory functions and dual effects on tumor progression. J Pathol 2020;250:555–72.
26. Wen SW, Lima LG, Lobb RJ, Norris EL, Hastie ML, Krumeich S, et al. Breast cancer-derived exosomes reflect the cell-of-origin phenotype. Proteomics 2019;19:e1800180.
27. Jana S, Li W, Lei PJ, Wang Z, Kibara S, Huang P, et al. Isolation and characterization of a novel mammary adenocarcinoma, MCa-P1362, with hormone receptor expression, human epidermal growth factor receptor 2 positivity, and enrichment in cancer and mesenchymal stem cells. Am J Pathol 2024;194:1137–53.

28. Verghese ET, Shenoy H, Cookson VJ, Green CA, Howarth J, Partanen RH, et al. Epithelial-mesenchymal interactions in breast cancer: evidence for a role of nuclear localized beta-catenin in carcinoma-associated fibroblasts. Histopathology 2011;59:609–18.
29. Verghese ET, Drury R, Green CA, Holliday DL, Lu X, Nash C, et al. MiR-26b is down-regulated in carcinoma-associated fibroblasts from ER-positive breast cancers leading to enhanced cell migration and invasion. J Pathol 2013;231:388–99.
30. Trajkovic K, Hsu C, Chiantia S, Rajendran L, Wenzel D, Wieland F, et al. Ceramide triggers budding of exosome vesicles into multivesicular endosomes. Science 2008;319:1244–7.
31. Louie DAP, Liao S. Lymph node subcapsular sinus macrophages as the frontline of lymphatic immune defense. Front Immunol 2019;10:347.
32. Pucci F, Garris C, Lai CP, Newton A, Pfirschke C, Engblom C, et al. SCS macrophages suppress melanoma by restricting tumor-derived vesicle-B cell interactions. Science 2016;352:242–6.
33. Liu CY, Battaglia M, Lee SH, Sun QH, Aster RH, Visentin GP. Platelet factor 4 differentially modulates $CD4^+CD25^+$ (regulatory) versus $CD4^+CD25^-$ (non-regulatory) T cells. J Immunol 2005;174:2680–6.
34. Harris GM, Raitman I, Schwarzbauer JE. Cell-derived decellularized extracellular matrices. Methods Cell Biol 2018;143:97–114.
35. Abusamra AJ, Zhong Z, Zheng X, Li M, Ichim TE, Chin JL, et al. Tumor exosomes expressing Fas ligand mediate $CD8^+$ T-cell apoptosis. Blood Cells Mol Dis 2005;35:169–73.
36. Maybruck BT, Pfannenstiel LW, Diaz-Montero M, Gastman BR. Tumor-derived exosomes induce $CD8^+$ T cell suppressors. J Immunother Cancer 2017;5:65.
37. Lebbink RJ, de Ruiter T, Adelmeijer J, Brenkman AB, van Helvoort JM, Koch M, et al. Collagens are functional, high affinity ligands for the inhibitory immune receptor LAIR-1. J Exp Med 2006;203:1419–25.
38. Vivinus-Nebot M, Ticchioni M, Mary F, Hofman P, Quaranta V, Rousselle P, et al. Laminin 5 in the human thymus: control of T cell proliferation via alpha6beta4 integrins. J Cell Biol 1999;144:563–74.
39. Liu X, Qiao Y, Chen J, Ge G. Basement membrane promotes tumor development by attenuating T cell activation. J Mol Cell Biol 2022;14:mjac006.
40. Chen Y, McAndrews KM, Kalluri R. Clinical and therapeutic relevance of cancer-associated fibroblasts. Nat Rev Clin Oncol 2021;18:792–804.